Describing Cro-Magnon: The femora, tibiae and fibulae

Erik Trinkaus, Vitale Sparacello, Song Xing, Adrien Thibeault, Sébastien Villotte

Describing Cro-Magnon: The Femora, Tibiae and Fibulae

Erik Trinkaus,[a,b,c*] Vitale S. Sparacello,[d] Song Xing,[e] Adrien Thibeault,[f] and Sébastien Villotte[g,h]

[a] Department of Anthropology, Washington University, Saint Louis, MO 63130, USA.

[b] 32 Cliff Street, Burlington, VT 05401, USA.

[c] Department of Anthropology, University of Vermont, Burlington, VT 05405, USA.

[d] Department of Life and Environmental Sciences, University of Cagliari, CA 09042, Italy

[e] Key Laboratory of Vertebrate Evolution and Human Origins of Chinese Academy of Sciences, Institute of Vertebrate Paleontology and Paleoanthropology, Chinese Academy of Sciences, Beijing 100044, China.

[f] UMR 5199, PACEA, Université de Bordeaux, CNRS, 33615 Pessac, France.

[g] UMR 7206 Éco-Anthropologie, équipe ABBA, CNRS, MNHN, Université de Paris, 75116 Paris, France

[h] Operational Directory Earth and History of Life, Royal Belgian Institute of Natural Sciences, Brussels, Belgium.

* Corresponding author

The authors declare no conflicts of interest.

Author contributions:

Erik Trinkaus: Conceptualization, Data curation, Investigation, Methodology, Visualization, Writing - original draft. **Vitale S. Sparacello**: Conceptualization, Data curation, Investigation, Methodology, Visualization, Writing - original draft. **Song Xing**: Data curation, Investigation, Methodology, Visualization, Writing - original draft. **Adrien Thibeault**: Methodology, Visualization, Writing-review & editing. **Sébastien Villotte**: Conceptualization, Funding acquisition, Investigation, Project administration, Resources, Writing - original draft.

Corresponding author: Erik Trinkaus

trinkaus@wustl.edu; 32 Cliff Street, Burlington ,VT 05401, USA

Abstract

As part of a reassessment of the Mid Upper Paleolithic human remains from Cro-Magnon (Dordogne, France), a morphological description and paleobiological consideration of the Cro-Magnon lower limb long bone (femoral, tibial and fibular) remains is presented. Following the reassociation of the lower limb remains (Thibeault and Villotte, 2018, J. Archaeol. Sci. Rep. 21, 76-86), the preserved bones are presented in terms of the Alpha (Cro-Magnon 1), Beta and Gamma older adult individuals.

Morphologically the Cro-Magnon femora, tibiae and fibulae fall comfortably within the ranges of variation of other earlier (Early and Mid) Upper Paleolithic human remains in most aspects. Their diaphyseal discrete morphologies follow the early modern human pattern of clear femoral pilasters and large gluteal buttresses, discrete tibial pilasters, and prominent tibial and fibular longitudinal sulci. Their femoral diaphyses exhibit levels of hypertrophy similar to those of other Late Pleistocene remains, although the Alpha and Beta ones are among the most robust, and Gamma is more gracile. The primary contrasts are in their body proportions, in that Alpha and Beta appear to have had linear proportions overall, yet Alpha and Gamma exhibit the low crural proportions usually associated with stocky bodies. As such, the Cro-Magnon lower limb remains both reinforce the E/MUP patterns but also extent the ranges of variation for the sample. These morphological aspects are joined by minor, age-related lesions in Beta and Gamma, but they are associated with a prominent femoral lesion and multiple other abnormalities (principally enthesopathies) in Alpha. The latter are likely part of a systemic disorder in Alpha (Cro-Magnon 1) of uncertain etiology.

Key Words:

Upper Paleolithic, Europe, Late Pleistocene, Femur, Tibia, Paleopathology, Diaphysis

1. Introduction

The Cro-Magnon rock shelter (Les Eyzies-de-Tayac-Sireuil, Dordogne, France) is one of the premier Upper Paleolithic sites, best known for establishing in 1868 the contemporaneity of early modern humans with Upper Paleolithic assemblages and Pleistocene fauna (Lartet, 1868; Broca, 1868). Although the human skeletal assemblage from the site was described in variable detail by Broca (1868) and Pruner-Bey (1868), and reassessed 100 years later by Vallois and Billy (1965) and Dastugue (1967), these human remains from Cro-Magnon have remained poorly known despite the incorporation of data from them into Late Pleistocene comparative analyses. In this context, and in the framework of a broader refocus on western Eurasian Upper Paleolithic human paleobiology, we have undertaken the reassessment of the Cro-Magnon human remains (Villotte and Balzeau, 2018; Thibeault and Villotte, 2018; Partiot et al., 2020; Villotte et al., 2020; Trinkaus et al., 2021a, 2021b).

The relatively abundant human remains represent all portions of the skeleton. However, they became commingled, whether *in situ* or subsequently, resulting in previous attempts to re-associate them by individual (e.g., Broca, 1868; Pruner-Bey, 1868; Vallois and Billy, 1965; Gambier et al., 2006). More recently, it has become evident that there are four adult individuals represented by the remains (Vallois and Billy, 1965; Thibeault and Villotte, 2018; Villotte et al., 2020; Trinkaus et al., 2021a, 2021b). To avoid confusion with the numbered craniofacial remains (see Vallois and Billy, 1965) and given the uncertainties of association between the appendicular remains and the cephalic elements (Trinkaus et al., 2021a), the four identified appendicular individuals are designated Alpha, Beta, Gamma and Delta (Thibeault and Villotte, 2018; Villotte et al., 2020). Only the first three of these postcranial individuals are evident in the lower limb bones, and only Alpha can be reliably associated with a craniofacial individual (Cro-Magnon 1) (Thibeault and Villotte, 2018; Trinkaus et al., 2021a).

In this contribution to the reassessment of the Cro-Magnon assemblage, we focus on the paleobiology of the femora, tibiae and fibulae of Alpha, Beta and Gamma. The more complete femora and tibiae have received attention since their partial descriptions by Broca (1868) and Pruner-Bey (1868), Vallois and Billy (1965) provided a limited set of osteometrics and morphological observations for most of the elements, and additional measures have been provided more recently (e.g., Trinkaus and Ruff, 2012). Yet, these fourteen earlier Upper

Paleolithic bones have never been described at an appropriate level of detail. Building on the associations of them by Thibeault and Villotte (2018), we provide such an assessment here.

2. Materials and Methods

2.1 The Cro-Magnon Leg Remains

The human remains from the Cro-Magnon are curated in the Musée de l'Homme, Muséum national d'Histoire naturelle (MNHN), Paris. The specimens of consideration here consist of eight partial femora (Cro-Magnon [CM] 4321 to 4329), four tibiae (CM 4330 to 4333, of which CM 4330 is essentially complete), and two fibulae (CM 4334 and CM 4335). Additional data derive from the associated pelvic remains. Data were collected in the Musée de l'Homme in 1980 (ET), 2008 (SV) and 2018 (SV and ET). As noted, these leg bones can be attributed to three appendicular individuals, Alpha, Beta and Gamma (Table S1). They are pelvically sexed as male, female and male respectively and aged as older adults based on auricular surface metamorphosis (Gambier et al., 2006; Thibeault and Villotte, 2018). They are referred to by either their catalog (CM) numbers for individual elements or Greek letter names for associated elements.

The human remains from Cro-Magnon were formerly attributed to the "Aurignacian" *sensu lato* (e.g., Vallois and Billy, 1965; Movius, 1969). They are now dated to an early phase of the Gravettian technocomplex (33–31,000 cal BP), part of the Mid Upper Paleolithic (MUP) (Henry-Gambier, 2002; Henry-Gambier et al., 2013).

2.2 Comparative Samples

Comparisons of the Cro-Magnon remains are made principally to western Eurasian (European and western Asian) Mid (MUP) and Early (EUP) Upper Paleolithic remains (E/MUP when pooled). Additional data from Late Upper Paleolithic humans (LUP), Middle Paleolithic modern humans (MPMH) and Late Pleistocene Neandertals provide a broader framework (SI 5). In the morphometric assessments, data are from personal measurement of the original bones and/or primary published descriptions of the paleontological remains. The comparative data for the cross-sectional geometric comparisons derive from personal research supplemented with data from Holt (1999), Stock et al. (2005), Mussini (2011), Puymerail et al. (2012), Villotte et al. (2017) and Cremasco et al. (2021) (see Trinkaus and Ruff, 2012; Xing et al., 2020). The contours

for the femoral geometric morphometric analyses are from personal research, published contours and B. Holt (pers. comm.).

2.3 Methods

The reassessment of these remains is based on visual observation of the original remains in the Musée de l'Homme in 2018 (ET and SV), combined with measurements taken in 1980 (ET) and 2008 (SV) and those provided by Vallois and Billy (1965). Microtomodensitometric (μCT) data for these bones were acquired at the AST-RX platform in the MNHN. They were obtained with the microfocus tube of the μCT scanner "v|tome|xL 240" (GE Sensing and Inspection Technologies Phoenix X ray). Each final volume was then reconstructed with isotropic voxels using NRecon v2.0 (Bruker microCT) in 16-bit format. Surface rendering of these 3D models was obtained with Avizo v.9 (Visualization Sciences Group Inc.).

2.3.1 Osteometrics

Osteometrics principally follow the Martin system (Bräuer, 1988), with additional measurements as defined in Trinkaus et al. (2014). For individuals providing bilateral measurements, the values were averaged prior to the comparisons. Summary statistics for comparative samples are provided as: (mean ± standard deviation, n). The quantitative comparisons were done using NCSS (2016).

2.3.2 Cross-Sectional Geometry

The cross-sectional geometry (CSG) data for the femora and tibiae (Tables S3 and S7) derive from 3D models of the Cro-Magnon bones. They were virtually positioned following Ruff (2019) when complete, and in the remaining cases the positioning and section levels were approximated by comparing fragments with other E/MUP and LUP virtual models with similar morphology and dimensions. Cross-sections were extracted at 50% and 80% of biomechanical length (Ruff, 2019) for the femora and at 50% for the tibiae, using Netfabb Standard 2018 for PC (© Autodesk 2017). CSG properties (cross-sectional areas and second moments of area) were calculated using a version of the program SLICE (Nagurka and Hayes, 1980) adapted as a macro routine inserted in Scion Image release Beta 4.03. Section moduli were computed from second moments of area following Trinkaus and Ruff (2012) (Tables S3 and S7).

To appropriately scale measures of diaphyseal strength (section moduli) across individuals, they were compared to the product of biomechanical length (to approximate beam

length) and body mass (to represent the baseline load on the lower limb). Body masses were estimated following Ruff et al. (2018) from femoral head diameters for all but Shanidar 2, for whom it was estimated from tibial plateau breadth.

2.3.3 Diaphyseal Geometric Morphometrics

The Cro-Magnon femora, especially those of Alpha (Cro-Magnon 1), are notable for the prominence of their pilasters and gluteal buttresses, as has been noted since Broca (1868) and Pruner-Bey (1868). To explore diaphyseal shape variation, in addition to assessments using perpendicular diameters and second moments of area, two-dimensional (2D) geometric morphometric (GM) analyses were performed on the 50% and 80% cross-sectional subperiosteal contours. GM analysis relies on superimposition (translation, scale and rotation) to eliminate non-shape information related to size, position and orientation (Zelditch et al., 2004). Standard generalized least squares (GLS) was used for the superimposition by minimizing the sum of squared distances between corresponding points on two configurations (Zelditch et al., 2004; Slice, 2005).

Along the 50% cross-sectional contour, a landmark [Type 2 of Bookstein (1991)] was defined at the most posterior point of the linea aspera (Fig. S32). In the cases in which the linea aspera is broad and flat, the landmark was located at the lateral ridge. In addition to the landmark, forty-nine equidistant semi-landmarks were then defined on each contour of a 50% cross-section. In the 80% cross-section, the contour was divided into equidistant parts and the 50 dividing points were defined as semi-landmarks (Fig. S32). The effect of arbitrary spacing of curve semi-landmarks was removed by the sliding technique (Gunz & Mitteroecker, 2013). The definitions of the landmark or semi-landmarks and the extraction of coordinates were carried out with TpsDig2 v. 2.12 (Rohlf, 1998).

The Geomorph package v. 3.2.1 (Adams et al., 2020) in R v. 3.5 (R Core team, 2020) was used to perform the Procrustes superimposition on the raw coordinates generated in TpsDig2 v. 2.12 (Rohlf, 1998), and the principal component analysis (PCA) of shape variables. PC1 and PC2 were used in the scatterplot to display the shape relationships among the different specimens. The criterion of minimizing the bending energy was also used when sliding the semi-landmarks (Zelditch et al., 2004; Adams et al., 2020), which produced very similar results as those of minimizing the Procrustes distance (compare Figs. 9 and 10 to Figs. S33 and S34).

When the contours for both right and left femora of an individual were available, we included them separately in the graphic comparisons.

Figure 1. Posterior (left) and medial (right) views of the CM 4322 (Gamma) and CM 4325 (Alpha) left femora. Scale: 7 cm.

3. Results

3.1 Body Size and Proportions

The overall body sizes of the Cro-Magnon individuals are best indicated by their femoral lengths [as predictors of stature (Feldesman et al., 1990)] and femoral head diameters (as predictors of body mass (Ruff et al., 2018)]. In terms of femoral lengths, Alpha and Gamma are among the taller of the E/MUP individuals, but they are exceeded by the very tall Barma Grande 2 and Grotte-des-Enfants 4 males and, to a lesser extent, Dolní Věstonice 14 and Sunghir 1 (Figs. 3 and S31). The bicondylar lengths of the Alpha and Gamma femora (≈486.2/490.0 and ≈475.5 mm respectively) closely bracket the E/MUP male mean (482.3 ± 29.1 mm, n = 11), and they are above the LUP distribution and all but one Neandertal (Amud 1). The Beta femoral length (≈454.7 mm) is only modestly shorter, above the E/MUP female mean (438.9 ± 31.5 mm, n = 11), but nonetheless exceeded by those of the Caviglione 1, Ostuni 1 and Veneri 2 females.

Figure 2. Anterior (left) and posterior (right) views of the CM 4330 (Gamma, left) and CM 4332 (Alpha, right) tibiae. Scale: 7 cm.

The femoral head diameters for Alpha and Gamma (≈46.7/48.6 and ≈49.4 mm respectively) similarly bracket the E/MUP male mean (49.3 ± 3.1 mm, n = 12) and are well below some of the larger E/MUP values (Figs. 3 and S31). The Beta femoral head diameter (42.2 mm), in contrast to its length, is below the E/MUP female mean (45.7 ± 2.7, n = 10), it exceeds only those of Dolní Věstonice 3 and the LUP Oberkassel 2, and it is close to those of Předmostí 9 and the LUP Cap Blanc 1.

If the proportions of femoral head diameter to length (as a reflection of body linearity) are compared across these samples, the Neandertals are relatively stocky, the MPMH sample very linear, the E/MUP sample relatively linear, and the LUP sample closer to the Neandertal one (Fig. 4; see Holliday, 1997a). The Gamma proportions are well within the relatively linear E/MUP proportions, but the Alpha and Beta ones are along the "linear" margin of the E/MUP distribution. In contrast, the tibial to femoral length proportions [often quantified by the crural index (see Table S10)] of Alpha and Gamma (Fig. 4) place them separate from the E/MUP

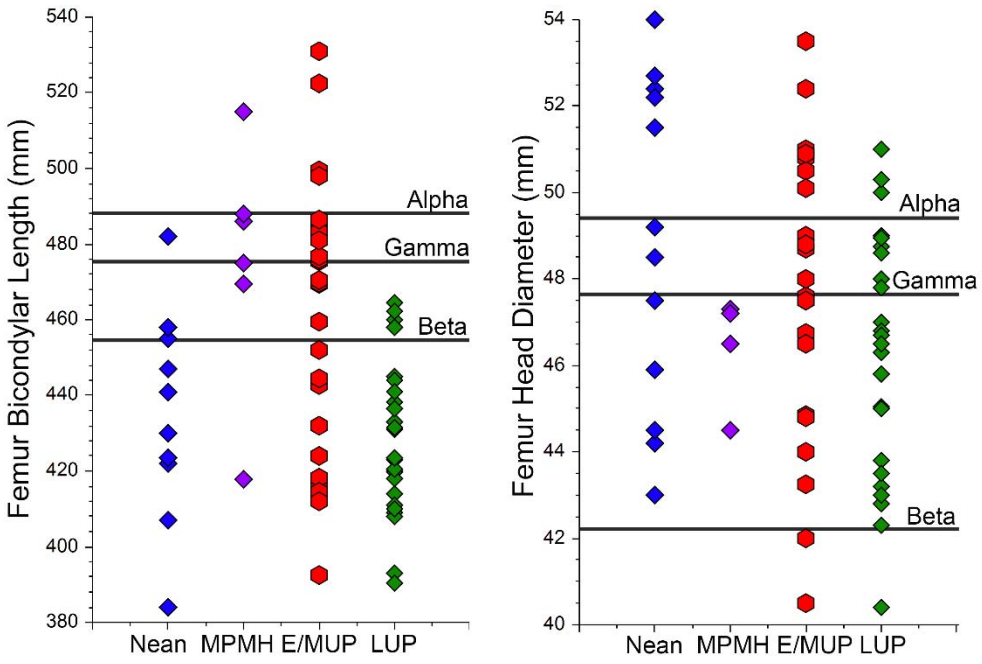

Figure 3. Comparisons of the femoral bicondylar lengths (as a proxy for stature) and femoral head diameter (as a proxy for body mass) of the Cro-Magnon individuals to those of comparative Late Pleistocene samples. Nean: Neandertals; MPMH: Middle Paleolithic modern humans; E/MUP: Early/Mid Upper Paleolithic humans; LUP: Late Upper Paleolithic humans.

distribution and with the relatively shorter tibiae and similar to the Neandertal distribution. They are also distinct from the LUP sample and especially the MPMH one. To the extent that low crural indices are associated with stocky body proportions (Holliday, 1997a, 1999), these tibiofemoral proportions contrast with the Cro-Magnon femoral head to length proportions, especially of Alpha. Relatively low tibiofemoral proportions are also present in the (albeit juvenile) E/MUP Lagar Velho 1 (Ruff et al., 2002), whose crural index should reflect what its adult value would have been (Cowgill et al., 2012). Such low tibiofemoral proportions are otherwise unknown among E/MUP individuals (Fig. 4).[1]

3.2 Epiphyseal Morphology

The epiphyses of the Cro-Magnon femora are largely unremarkable in their articular and musculoligamentous configurations. The CM 4322 femur does have a relatively high neck-shaft angle, ≈129°, which places it above most of the E/MUP (and Neandertal plus LUP) angles (Figs. 5 and S19). Only Dolní Věstonice 3 and Nahal Ein Gev 1 have higher angles, and it is well

above the E/MUP mean (119.8° ± 5.7°, n = 21). It is nonetheless low for a MPMH femur. Given that neck-shaft angles decrease with elevated proximal femoral loads during development (Anderson and Trinkaus, 1998), the CM 4322 value implies modest lower limb loads for a young Gamma. The neck-shaft angle of CM 4327 cannot be reliably measured, but the preserved portion of the medial neck indicates an angle similar to that of CM 4322 (Fig. S19).

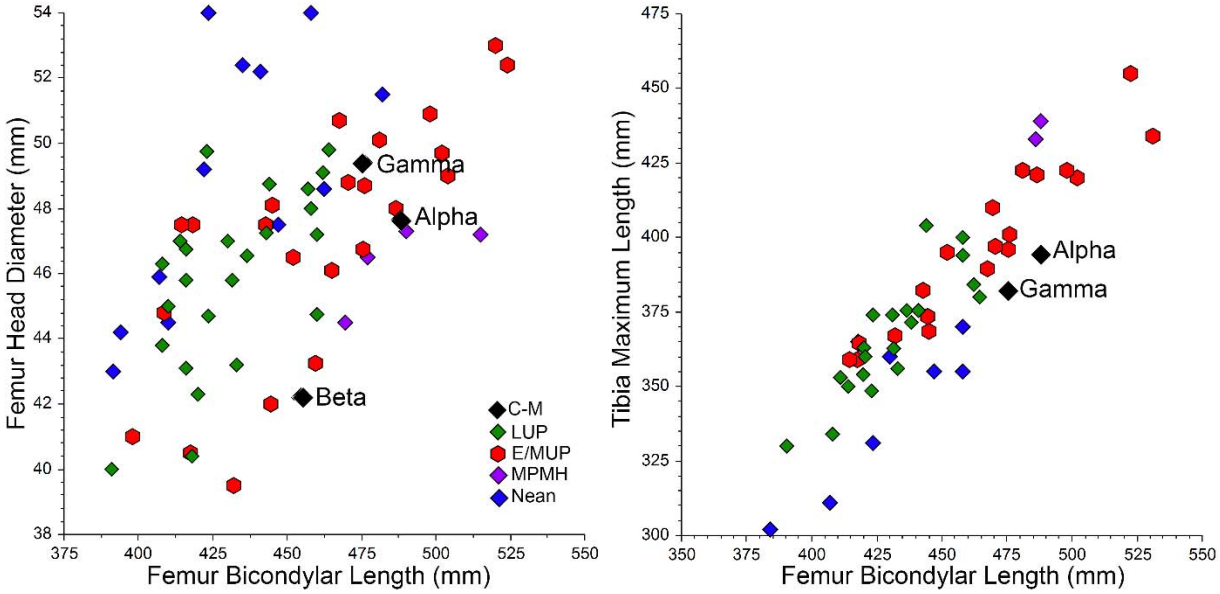

Figure 4. Femoral head diameter versus bicondylar length (as proxies for body mass and stature) (left) for Cro-Magnon individuals and comparative Late Pleistocene samples. Tibial versus femoral lengths (right) for Cro-Magnon individuals and comparative samples, reflecting distal to proximal leg segment proportions (as do crural indices). Abbreviations as in Fig. 3.

The tibial plateau of CM 4330 is notable only for its low retroversion angle in a Late Pleistocene context (Figs. 5 and S23). Its value of 10° is at the bottom of the E/MUP range of variation, matched only by Sunghir 1 and the (albeit pathological) Dolní Věstonice 15. As with the moderately high femoral neck-shaft angle, it implies moderate loads during development for Gamma (Trinkaus, 1975).

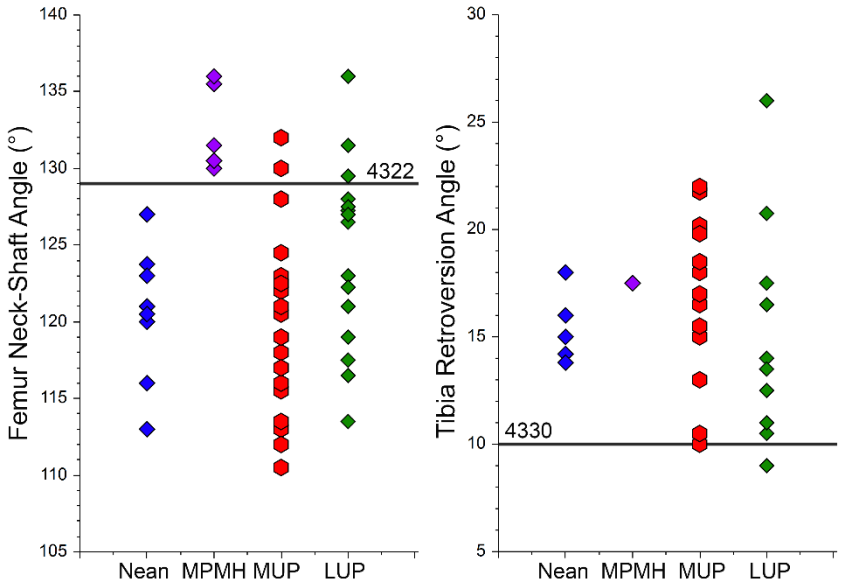

Figure 5. Comparisons of the Gamma femoral neck-shaft (CM 4322) and the tibial retroversion (CM 4330) angles to samples of Late Pleistocene humans. Abbreviations as in Fig. 3.

The two distal femora, CM 4328 and 4329, have bicondylar angles (7° and 9° respectively) that fall well within both recent human and Pleistocene *Homo* ranges of variation (Tardieu and Trinkaus, 1994, and references therein). In association with these angles, they have expanded lateral patellar surfaces and raised lateral patellar margins (Figs. S2 and S16). This configuration indicates normal developmental acquisition of leg posture and locomotion (Tardieu and Trinkaus, 1994; Cowgill et al., 2010).

Distally, the Gamma tibiae (CM 4330 and 4333) exhibit distinct lateral squatting facets (Figs. 6 and S29). Each one has a rounding of the anterolateral trochlear articular margin, extending 3.2 and 4.1 mm respectively from the trochlear margin. The one on CM 4330 articulates with the CM 4337 talus, and they join other indications of talocrural and subtalar hyperdorsiflexion (Trinkaus et al., 2021b). Neither the CM 4328 or CM 4329 distal femoral condyles exhibit posteroproximal flattening [femoral squatting facets (Trinkaus, 1975)].

Figure 6. Anterior views of the CM 4330 and 4333 distal tibiae. The arrows indicate the modest squatting facets. Scale bar: 5 cm.

3.3 Diaphyseal Morphology

The Cro-Magnon femoral and tibial diaphyses, and particularly those attributed to Cro-Magnon 1, have been noted since Broca (1868) and Pruner-Bey (1868) as being markedly pilastric and platycnemic [the latter a "lame de sabre" for Broca (1868)]. However, Vallois and Billy (1965) noted that they were rather less pilastric and platycnemic than originally described. In fact, the Cro-Magnon lower limb diaphyses exhibit considerable variation, despite sharing a suite of features common among E/MUP humans (Figs. 1, 2 and 7).

The Cro-Magnon femora, as with most E/MUP ones, exhibit prominent pilasters, exaggerated in CM 4327 and 4325 by bony growths along the linea aspera (Figs. 1 and 7). Along the midshafts the pilasters are largely flat medially but exhibit variably developed longitudinal sulci laterally (especially on CM 4325 and 4327). The pilastric indices for CM 4327, 4325, 4324 and 4322 (129.5, 125.3, 124.1 and 118.5 respectively) are above average but unexceptional for E/MUP femora (118.1 ± 11.1, n = 28) (Table S11). Their distribution of anteroposterior versus mediolateral second moments of area (Ix vs. Iy) (Fig. 8) places them well within the E/MUP (and LUP) distribution. In that comparison, CM 4327 is unusual for its size but not for its proportions, given a tendency for Ix to increase more rapidly than Iy with size, especially in highly mobile groups (Sparacello et al., 2018). Similarly, their relative positions in a geomorphometric analysis of their femoral midshaft contours (Fig. 9) align them at the pilastric end of the distribution, primarily distinct from the rounded contours of the Neandertals, and among the pilastric ones

with the more pronounced lateral pilastric sulci. These aspects, again, are most evident in the Alpha (CM 4325 and 4327) femora.

More proximally on the femoral diaphysis, all of the femora exhibit prominent lateral gluteal buttresses (Figs. 7, S8, S15 and S20). They are accentuated by marked sulci posteriorly, in the region of the gluteal tuberosity, and all but CM 4322 have shallow depressions anteriorly. CM 4327 has a relatively high meric index (83.2), indicating a rounder cross-section, but CM 4325, 4323 and 4322 have indices (76.5, 70.8 and 72.3) similar to other E/MUP femora (75.7 ± 6.8, n = 31) (Table S11). The same pattern is evident in their subtrochanteric perpendicular second moments of area (Imax vs. Imin) (Fig. 8), in which CM 4327 is on the rounder side of the E/MUP distribution but the other three femora are well within the E/MUP variation. In a geomorphometric analysis of their femoral proximal shaft contours, the two Gamma femora (CM 4322 and 4323) are among the E/MUP femora with more prominent lateral buttresses (Fig. 10). The Alpha femora are unusual in the Late Pleistocene context, in that they are both moderately round yet exhibit prominent gluteal buttresses.

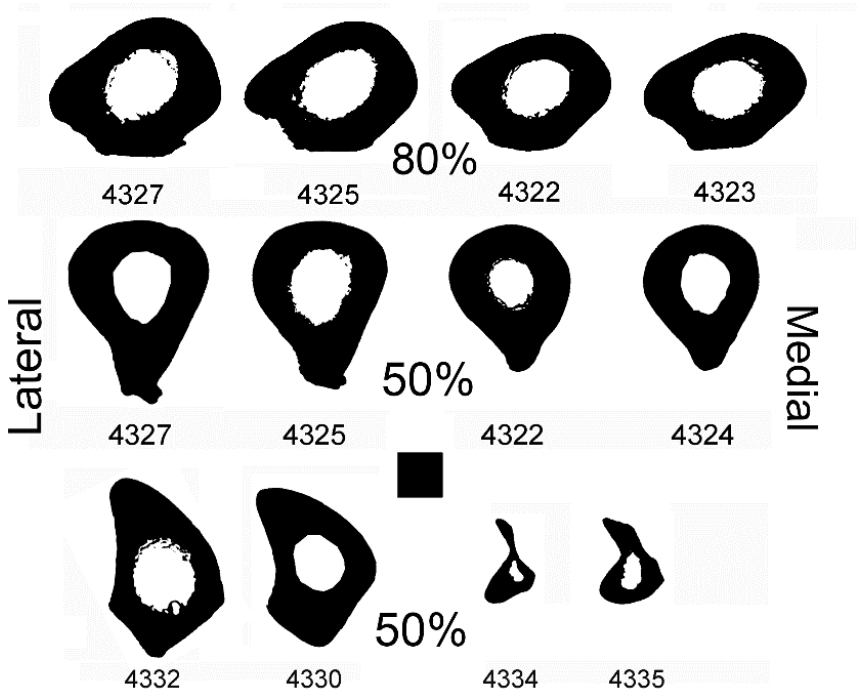

Figure 7. Cross-sections of the Cro-Magnon femora, tibiae and fibulae at the femoral subtrochanteric level (80%) and at midshaft (50%) for each of the bones. Scale box is 1 cm.

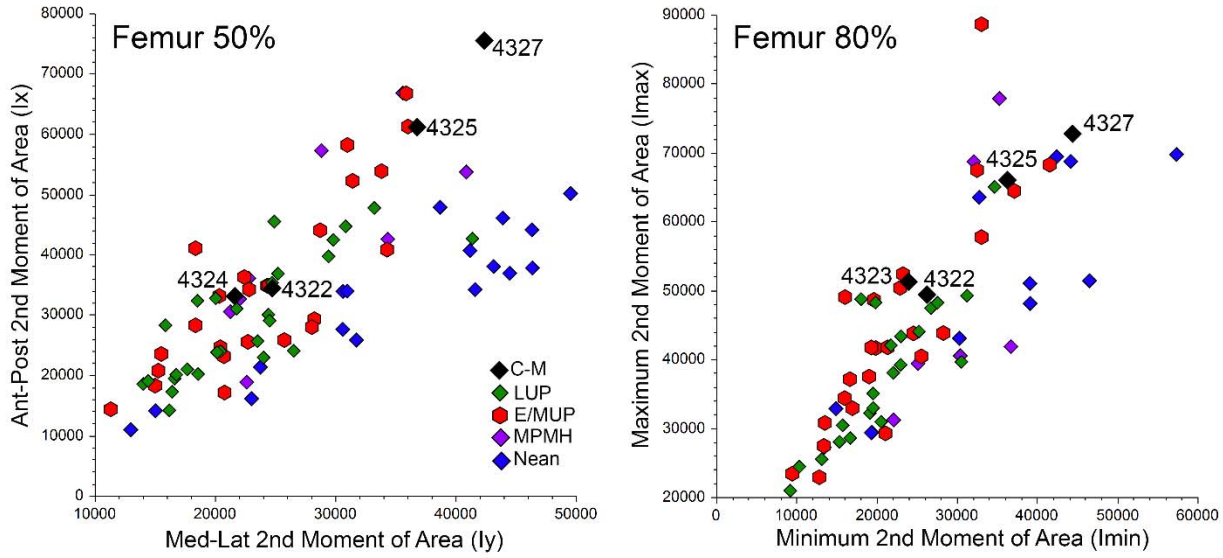

Figure 8. Perpendicular second moments of area for the Cro-Magnon femoral diaphyses and the comparative Late Pleistocene samples. Left: anteroposterior (Ix) versus mediolateral (Iy) midshaft (50%) second moments of area. Right: maximum (Imax; approx. mediolateral) versus minimum (Imin) subtrochanteric (80%) second moments of area. Abbreviations as in Fig. 3.

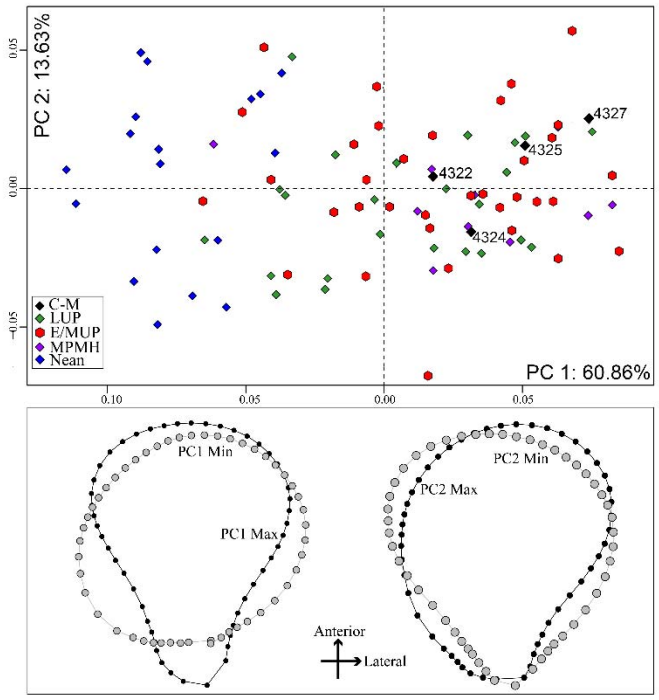

Figure 9. Femoral midshaft contour PC 1 versus PC 2 for the Cro-Magnon femora and the comparative Late Pleistocene samples. Abbreviations as in Fig. 3.

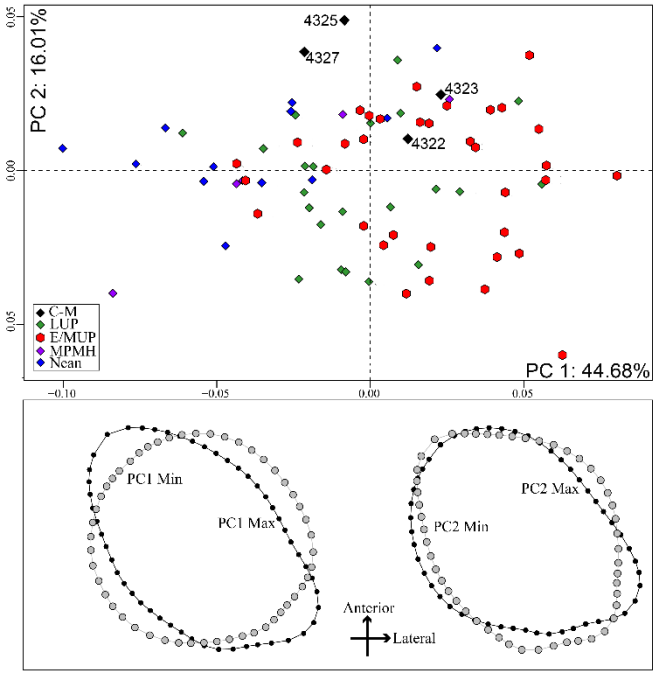

Figure 10. Femoral subtrochanteric contour PC 1 versus PC 2 for the Cro-Magnon femora and the comparative Late Pleistocene samples. Abbreviations as in Fig. 3.

The Cro-Magnon 4330 and 4332 tibial diaphyses exhibit well-formed concavities (or longitudinal sulci) of the lateral diaphysis between the anterior crest and the interosseus line, bordered by rounded anterior crests and sharp interosseus crests (Fig. 7). Similar configurations are evident on the less complete CM 4331 and 4333 midshaft to distal diaphyses. In this pattern they are similar to other early modern human tibiae and contrast with the more amygdaloid cross-sections of archaic *Homo* tibiae (Stringer et al., 1998; Churchill et al., 2000; Trinkaus, 2009). CM 4332 and especially CM 4330 combine this morphology with prominent tibial pilasters (Fig. S27), and the distal extent of one is evident on CM 4333. However, the cnemic indices of CM 4330 and 4332 (156.3 and 169.6) are unexceptional for an Upper Paleolithic tibia (E/MUP: 161.0 ± 14.5, n = 25), although the CM 4332 one is moderately high for a Middle Paleolithic tibia (Table S11). The same pattern is evident in comparisons of the Cro-Magnon mid-proximal (cnemic level) perpendicular diameters and the midshaft perpendicular second moments of area (Fig. 11). As noted by Vallois and Billy (1965), and *contra* Broca (1868) and Pruner-Bey (1868), there is little that is unusual in the Cro-Magnon tibial diaphyses for an Upper Paleolithic human.

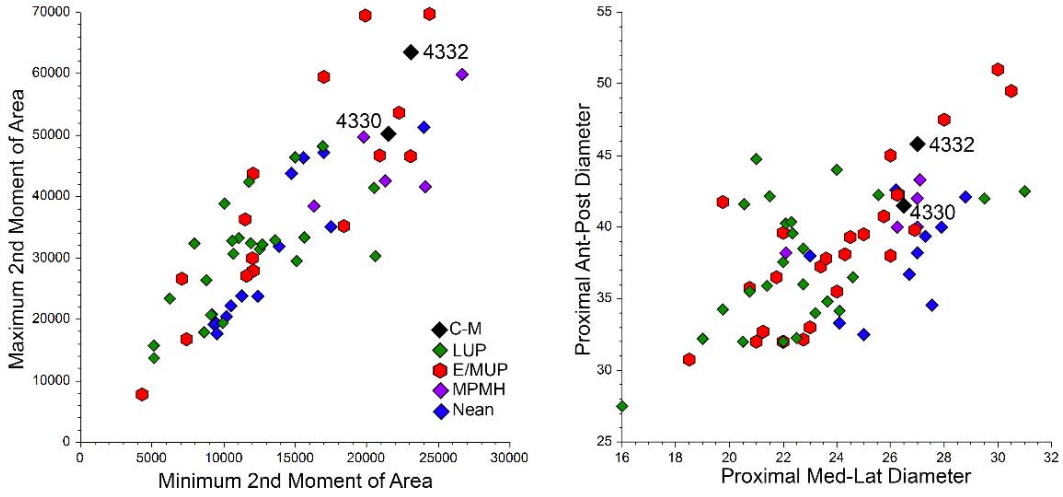

Figure 11. Diaphyseal proportions of the Cro-Magnon tibiae and those of the Late Pleistocene comparative samples. Left: midshaft maximum (≈ant.-post.) versus minimum (≈med.-lat.) second moments of area (Imax vs. Imin). Right: mid-proximal (cnemic level) anteroposterior versus mediolateral diameters. Abbreviations as in Fig. 3.

The fibular diaphyses from Cro-Magnon are similar to those of other Upper Paleolithic humans in exhibiting pronounced longitudinal sulci, especially laterally (Figs. 7 and S30; see Trinkaus, 2006; Trinkaus et al., 2014).

3.4 Lower Limb Hypertrophy

3.4.1 Femoral Diaphyses

The Cro-Magnon femora in particular may provide evidence of lower limb hypertrophy, beyond what would be expected for weight-bearing and locomotion in the context of Late Pleistocene humans. In a comparison of the femoral midshaft (50%) polar moment of area (as a reflection of overall bending and torsion strength (Ruff, 2019) to body mass times femur length (as reflections of the baseline load and beam length) (Fig. 12), the Cro-Magnon femora bracket the Late Pleistocene distribution. There is little difference across the Late Pleistocene samples, especially once the several layers of estimation in the analysis are taken into account (*contra* Rodríguez et al., 2018). The CM 4322 femur falls among the more gracile of the Late Pleistocene femora, but the CM 4324, 4325 and especially 4327 femora are among the more

robust of these long bones. CM 4327 stands out particularly, in part due to its large size, but it is at the limits of the Late Pleistocene variation in relative strength.

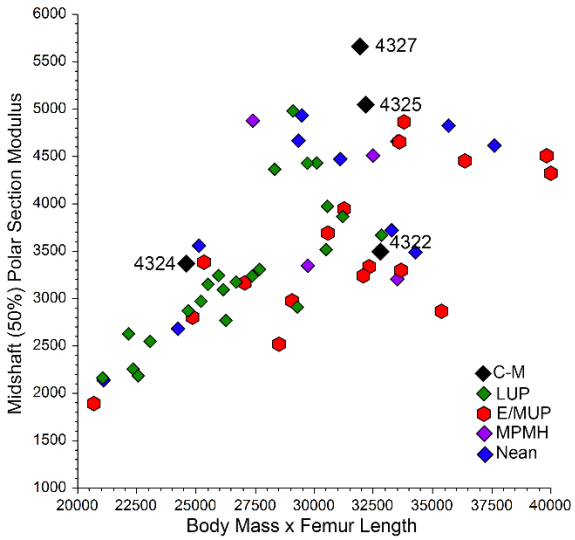

Figure 12. Femoral midshaft (50%) polar section modulus versus body mass times femur length, for the Cro-Magnon femora and comparative Late Pleistocene samples. Sample abbreviations as in Fig. 3.

However, the Alpha femora, and especially CM 4327, are pronounced in the sizes of their pilasters (Figs. 7 and 9) [although their midshaft proportions are as expected for large E/MUP femora (Fig. 8)]. If the midshaft mediolateral second moments of area are compared to body mass times femur length (Fig. 13), the relative positions of the CM 4322 and 4324 femora remain the same as with the polar moments of area, but the positions of the CM 4325 and 4327 femora become less pronounced (although still high for E/MUP femora). Yet, in the comparison of the 50% anteroposterior second moments of area to body mass times femur length (Fig. 13), CM 4325 is at the limits of the Late Pleistocene variation, and CM 4327 is exceptional in its relative anteroposterior strength [only the MPMH Qafzeh 9 comes close, and its femoral cross-section was partially reconstructed (Trinkaus and Ruff, 1999)].

It is therefore apparent that the Cro-Magnon femora exhibit a large range of diaphyseal hypertrophy, from the relatively gracile CM 4322 to the unusually robust CM 4327. As noted by Broca (1868), the Cro-Magnon 1 femoral diaphyses were strongly developed, but [as noted by Vallois and Billy (1965)] the Cro-Magnon 1 femora do not represent the full sample.

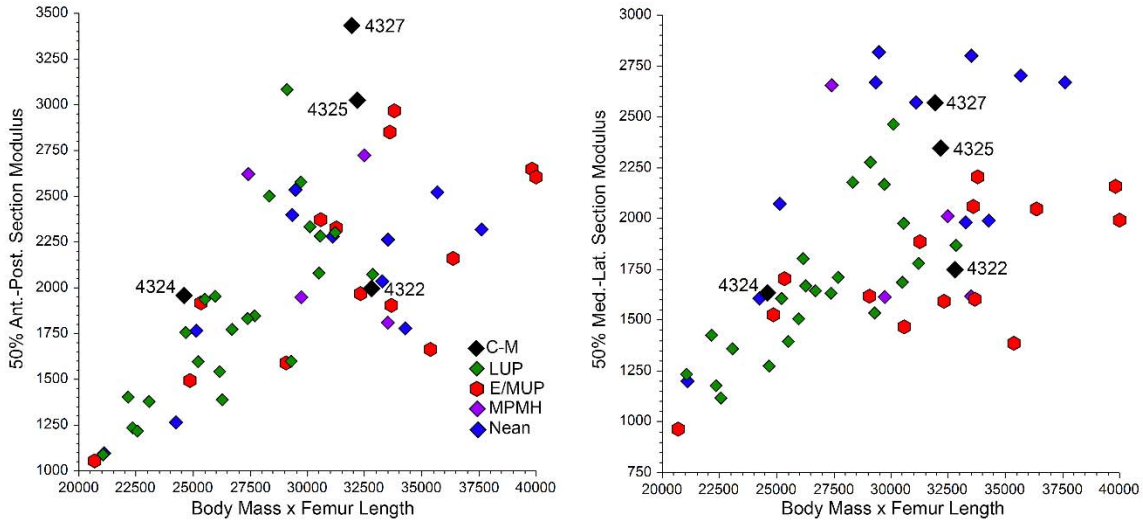

Figure 13. Femoral midshaft (50%) anteroposterior (left) and mediolateral (right) section moduli versus body mass times femur length, for the Cro-Magnon femora and comparative Late Pleistocene samples. Sample abbreviations as in Fig. 3.

3.4.2 Gluteal Tuberosities

All five of the Cro-Magnon femora exhibit large and variably rugose gluteal tuberosities located in (subtrochanteric) sulci posterior of the lateral (gluteal) buttress (Fig. 14; see Figs. S8, S15 and S20). None of them exhibits third trochanters [*contra* Vallois and Billy (1965)]. The breadths of the Cro-Magnon tuberosities (10.5 – 12.9 mm, 11.9 ± 1.0 mm, n = 5) are above most of those for E/MUP femora (Fig. 15; 5.0 – 14.2 mm, 10.0 ± 2.3 mm, n = 13). They are exceeded only by the large Baousso da Torre 1 value. More appropriately, if the dimension of the gluteal tuberosity reflects the size of that portion of the gluteus maximus muscle which inserts into it (the remainder inserting into the iliotibial tract), it should be scaled against body mass (reflecting the baseline load) and femoral length (reflecting its load arm). The resultant distribution (Fig. 15) places the CM 4322 and 4325 among the E/MUP femora, CM 4323 and 4327 at the top of the E/MUP distribution, and CM 4324 (with its large tuberosity and smaller body size) at the robust limits of the Late Pleistocene sample. To the extent that this one discrete muscular insertion area reflects lower limb hypertrophy, the Cro-Magnon femora are among the more robust of the E/MUP ones.

Figure 14. Posterolateral views of the gluteal tuberosities of the Cro-Magnon femora. CM 4322, 4324 and 4325 are left. CM 4323 and 4327 are right and have been reversed. Scale bar: 5 cm.

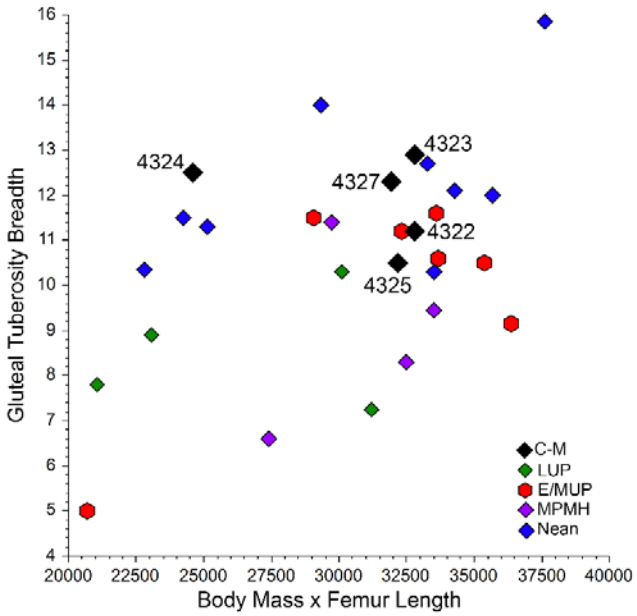

Figure 15. Bivariate plot of gluteal tuberosity breadth, as a measure of the hypertrophy of the gluteus maximus muscle, versus body mass times femur length, as measures of baseline load and load arm. Sample abbreviations as in Fig. 3.

3.5 Paleopathology

3.5.1 Alpha (Cro-Magnon 1) Abnormalities

The primary lesion on the Cro-Magnon lower limb long bones is a large abnormality on the anterolateral distal diaphysis of the CM 4325 (Alpha; Cro-Magnon 1) femur (Figs. 16 and

S12). It was noticed in 1868 and attributed to interpersonal aggression trauma by Broca (1868) or to either trauma or localized inflammation by Pruner-Bey (1968). A century later, Dastugue (1967) rejected a traumatic origin of the lesion and considered it to be from an adjacent soft tissue abnormality, part of a systemic condition that also produced lytic lesions on the frontal squamous portion and the anterosuperior left ilium (Fig. S13). Abnormalities of the Alpha right metatarsal 4 and 5 heads and his hallucal proximal phalanx head may also be part of the same systemic condition (Trinkaus et al., 2021b).

Figure 16. Anterior view of the CM 4325 (Alpha) left femur with the location of the lesion indicated (left) and anterolateral detailed view of the lesion (right). Scale bars: 5 cm.

The primary area of the femoral lesion consists of ovoid area of raised cortical bone with a raised anterior margin exhibiting microporosity but a posterior margin that blends into the adjacent subperiosteal bone. There is a less pronounced area that extends proximally, to an overall lesion height of ≈56 mm and a breadth of ≈30 mm. Within the ovoid portion there is an approximately circular depression ≈21 mm in diameter, with anterior microporosity and a circular pit limited to the cortical bone. The ultimate etiology of the femoral lesion is unclear, but it is likely, as suggested by Dastugue (1967), to be part of a systemic condition affecting soft tissue which impinged on the subperiosteal bone locally.

In addition, both femora attributed to Alpha (Cro-Magnon 1) exhibit enthesopathies in the areas of the gluteal tuberosity, the spiral line, and the midshaft linea aspera (Figs. 14, S6 and

S8 to S11). The bony growths are most pronounced on the CM 4327 right femur, developing into small knobs of bone on the spiral line, the mid-gluteal tuberosity and the linea aspera. Both femora have small protuberances at the proximal ends of their gluteal tuberosities (Figs. 14 and S8), which were considered incipient third trochanters by Vallois and Billy (1965); they are best considered further manifestations of these enthesopathies.

More distally, the CM 4331 (Alpha) left tibia has a large knob of bone, extending ≈9 mm posterolaterally from the distal epiphysis (Fig. S28). It did not affect the trochlear facet or the more proximal tibiofibular syndesmosis, and it was likely an ossification of the posterior tibiofibular ligament.

3.5.2 Beta Abnormalities

The lesions on the Beta femora (Figs. S14 and S16) consist of minor periarticular osteophytic swellings, a bony reaction adjacent to the proximoposterior medial condyle related to the insertion of the gastrocnemius medial head, and a depressed area of the distoposterior medial condyle. The last lesion has a smooth floor, lacks foramina, and is probably an osteochondritis dissecans; it resembles the changes seen on the CM 4294 and 4295 distal humeri, also attributed to Beta (Villotte et al., 2020).

3.5.3 Gamma Abnormalities

The femoral, tibial and fibular remains attributed to Gamma exhibit only very minor entheseal changes and periarticular irregularities.

4. Discussion

4.1 Morphological Aspects

The Cro-Magnon Alpha, Beta and Gamma femoral, tibial and fibular remains exhibit a suite of morphological features that encompass most of the variation evident in the E/MUP comparative sample. In terms of basic epiphyseal and diaphyseal morphology, they share with other E/MUP remains strong femoral gluteal buttresses, clear femoral and tibial pilasters, and strong tibial and especially fibular longitudinal sulci. In agreement with their pedal remains, at least the Gamma tibiae provide further evidence of habitual squatting. Yet within these patterns, there is considerable variation within the Cro-Magnon sample.

In terms of body proportions (Fig. 4), Alpha and Beta appear linear with modest implied body masses (femoral heads) relative to their statures (femoral lengths), as do most E/MUP

remains (Holliday, 1997a). Gamma is less linear, but both Alpha and Gamma have short tibiae relative to their femora (or low crural indices), at or beyond the limits of the E/MUP variation and among those of the Neandertals. In ecogeographical terms, the former aspect implies subtropical proportions and has been used to infer substantial gene flow into Europe with the western Eurasian establishment of early modern humans (Holliday, 1997a). In contrast, the latter implies cold adaptations (Trinkaus, 1981; Holliday, 1997b) and (along with similar proportions in Lagar Velho 1) supports Neandertal-to-modern human gene flow within Europe (Trinkaus and Zilhão, 2002; see also Holliday, 1999; Trinkaus, 2007); by the same criteria the high crural indices of most E/MUP remains have been used to infer gene flow into Europe with the appearance there of early modern humans (Trinkaus, 1981; Holliday, 1997a).

The Alpha femora are notable for their large and prominent pilasters (Figs. 7 and 9). Yet, as is evident in Fig. 8, its femoral midshaft proportions are as expected for Upper Paleolithic femora with their large dimensions (see Sparacello et al., 2018). At the same time, the Beta and Gamma femora have more modest pilasters, with femoral midshaft proportions commensurate with their diaphyseal dimensions. Despite an emphasis on the Alpha pilasters since Broca (1868) and Pruner-Bey (1868), what are of note are the large dimensions of the Alpha femoral diaphyses (Fig. 12). In the same context, the Alpha femora also exhibit unusually prominent gluteal buttresses (Fig. 10), yet their subtrochanteric proportions are unexceptional for Upper Paleolithic femora of their size (Fig. 8).

When the diaphyseal structural properties are appropriately scaled to baseline loads (body mass) and beam length (bone length), the Alpha and Beta femora are among the most robust of the Late Pleistocene femora and the most robust of the E/MUP ones (Fig. 12). The Gamma femur, in contrast, falls among the less reinforced E/MUP femora [and its femoral neck-shaft and tibial retroversion angles suggest modest loads during development (Fig. 5)]. This hypertrophy pattern holds when their anteroposterior diaphyseal strengths are appropriately scaled (Fig, 13), but the Alpha and especially Beta femora are less pronounced in their relative mediolateral strengths. All of the Cro-Magnon femoral structural properties are compatible with high levels of terrestrial mobility in a rough terrain, as has been proposed in various studies (Holt, 1999; Shackelford, 2007; Ruff et al., 2015; Villotte et al., 2017; Sparacello et al., 2018) for Upper Paleolithic remains.

4.2 Paleopathology

The changes evident on the Beta and Gamma leg remains are all minor and expected given their relatively advanced ages-at-death (Gambier et al., 2006). Some of the enthesopathies of the CM 4325 and 4327 (Alpha) femora could also be attributed to his older age-at-death. However, the extent to which there are (especially on CM 4327) discrete bony growths along the proximal femoral muscular attachments and along the midshaft linea aspera, combined with the large ossification of his left distal tibiofibular ligament, suggests that that Alpha suffered from more than age-related connective tissue ossifications. If these changes are combined with the CM 4325 distal femoral diaphyseal lesion, plus the changes elsewhere in the skeleton, it is evident that a systemic condition of genetic (Charlier et al., 2018), infectious (Dastugue, 1967), and/or idiopathic (Thillaud, 1981) origins was likely responsible for both the more pronounced lesions and a number of the minor changes.

These pathological changes in the Cro-Magnon remains, and especially those of Cro-Magnon 1 (Alpha), join a suite of developmental and degenerative abnormalities among Late Pleistocene humans (Wu et al., 2011; Trinkaus et al., 2014; Trinkaus, 2018; and specimen specific references in each). In particular, the systemic nature of the Cro-Magnon 1 lesions joins the E/MUP presence of systemic abnormalities (both developmental and degenerative) in the Barma Grande 2, Brno-Francouzká 2, Dolní Věstonice 15 and Sunghir 3 individuals, plus the non-European Nazlet Khater 2 and Tianyuan 1 (Churchill and Formicola, 1997; Schultz and Novaček, 2005; Trinkaus et al., 2006, 2014; Crevecoeur, 2008; Shang and Trinkaus, 2010). These cases, plus minor and major traumatic lesions in a number of individuals (Wu et al., 2011; Trinkaus et al., 2006, 2014), reflect both the risks and the survival of these Late Pleistocene individuals.

5. Conclusion

A paleobiological reassessment of the femoral, tibial and fibular remains from Cro-Magnon, attributed to three older adult individuals (Alpha, Beta and Gamma), places them comfortably among other human remains of the earlier (Early and Mid) Upper Paleolithic in most aspects. Their diaphyseal discrete morphologies follow the early modern human pattern of clear femoral pilasters and tibiofibular longitudinal sulci. Their femoral diaphyses exhibit levels of hypertrophy similar to other Late Pleistocene remains, although the Alpha and Beta ones are

among the most robust. The primary contrasts are in terms in body proportions, in that Alpha and Beta appear to have had linear proportions overall, yet Alpha and Gamma exhibit the low crural proportions associated with stocky bodies. As such, the Cro-Magnon leg remains both reinforce the E/MUP patterns but also extend the ranges of variation for the sample.

These aspects are joined by minor, age-related lesions in Beta and Gamma, but they are associated with a prominent femoral lesion and multiple other abnormalities in Alpha. The latter are likely part of a systemic disorder in Alpha (Cro-Magnon 1) of uncertain etiology.

6. Acknowledgments

The authors thank Veronique Laborde, Aurélie Fort (curators at the Musée de l'Homme) and Dominique Grimaud-Hervé (in charge of the collection) for granting access to the Cro-Magnon remains, and Aurélie Fort for the image of the Cro-Magnon catalog. Many colleagues and curators have provided access to Late Pleistocene comparative postcranial remains. T.W. Holliday provided helpful comments. To all we are grateful. Funding: This research was supported by ANR Gravett'Os (ANR-15-CE33-0004). The funding agency had no role in the research design or publication.

7. Footnote

[1] It is recognized that these body proportions are based on estimated values. However, the Beta head diameter is a direct measurement (Fig. S14), and that of Gamma is from completing a partial head contour (Fig. S17). The Alpha one is estimated more, but it is based on bilaterally well-preserved acetabula (Table S4). The Gamma tibial length is a direct measurement (Table S6; Fig. 2), and its femoral length is from a secure antimeric virtual reassembly (Fig. S18). The lengths of the Alpha and Beta femora and the former's tibia are less secure. Yet, the Alpha femora extend from their supracondylar areas to their distal necks (Figs. 1 and S1), its tibia is present from the supramalleolar area to the proximal tuberosity (Fig. S21), and the Beta femora elements provide a minimum length from the distal condyles to the greater trochanter (Fig. S3). Therefore, the leg proportions of Gamma can change little from those presented, and those of Alpha and Beta should be very close to their original values.

8. References

Anderson, J.Y., Trinkaus, E., 1998. Patterns of sexual, bilateral and inter-populational variation in human femoral neck-shaft angles. J, Anat. (Lond.) 192, 279-285.

Adams, D. C., Collyer, M. L., Kaliontzopoulou, A., 2019. Geomorph: Software for geometric morphometric analyses. R package version 3.1.0. https://cran.r-project.org/package=geomorph.

Bookstein, F., 1991. Morphometric tools for landmark data: Geometry and biology. Cambridge University Press, Cambridge.

Bräuer, G., 1988. Osteometrie. in: Knussman, R. (Ed.) Anthropologie I. Fischer, Stuttgart. pp. 160-232.

Broca, P., 1868. Sur les crânes et ossements des Eyzies. Bull. Soc. Anthropol. Paris 3, 350–392. https://doi.org/10.3406/bmsap.1868.9548

Charlier, P., Benmoussa, N., Froesch, P., Huynh-Charlier, I., Balzeau, A., 2018. Did Cro-Magnon 1 have neurofibromatosis type 1? Lancet 391, 1259.

Churchill, S.E., Formicola, V., 1997. A case of marked bilateral asymmetry in the upper limbs of an Upper Palaeolithic male from Barma Grande (Liguria), Italy. Intl. J. Osteoarchaeol. 7, 18-38.

Churchill, S.E., Berger, L.R., Parkington, J.E., 2000. A Middle Pleistocene human tibia from Hoedjiespunt, Western Cape, South Africa. S. Afr. J. Sci. 96, 367-368.

Cowgill, L.W., Warrener, A., Pontzer, H., Ocobock, C., 2010. Waddling and toddling: The biomechanical effects of an immature gait. Am. J. Phys. Anthropol. 143, 52-61. https://doi.10.1002/ajpa.21289.

Cowgill, L.W., Eleazer, C.D., Auerbach, B.M., Temple, D.H., Okazaki, K., 2012. Developmental variation in ecogeographic body proportions. Am. J. Phys. Anthropol. 148, 557-570. https://doi.10.1002/ajpa.22072.

Cremasco, M.M., D'Amore, G., Sparacello, V.S., Mussi, M., Galland, M., Profico, A., Masali, M., Di Marco, S., Miccichè, R., Friess, M., Sineo, L., 2021. Multi-proxy analysis suggests Late Pleistocene affinities of human skeletal remains attributed to Balzi Rossi. J. Anthropol. Sci. 99, 1-42. https://doi.10.4436/jass.99014.

Crevecoeur, I., 2008. Étude Anthropologique du Squelette du Paléolithique Supérieur de Nazlet Khater 2 (Égypte). Leuven University Press, Leuven.

Dastugue, J., 1967. Pathologie des hommes fossiles de l'Abri de Cro-Magnon. L'Anthropol. 71, 479-492.

Feldesman, M.R., Kleckner, J.G., Lundy, J.K., 1990. Femur/stature ratio and estimates of stature in mid- and late-Pleistocene fossil hominids. Am. J. Phys. Anthropol. 83, 359-372. https://doi.org/10.1002/ajpa.1330830309.

Gambier, D., Brůžek, J., Schmitt, A., Houët, F., Murail, P., 2006. Révision du sexe et de l'âge au décès des fossiles de Cro-Magnon (Dordogne, France) à partir de l'os coxal. C. R. Palevol 5, 735-741. https://doi.10.1016/j.crpv.2005.12.011.

Gunz, P., Mitteroecker, P., 2013. Semilandmarks: a method for quantifying curves and surfaces. Hystrix, Ital. J. Mammal., 24, 103-109. doi.10.4404/hystrix-24.1-6292.

Henry-Gambier, D., 2002. Les fossiles de Cro-Magnon (Les Eyzies-de-Tayac, Dordogne): nouvelles données sur leur position chronologique et leur attribution culturelle. Bull. Mém. Soc. Anthropol. Paris 14,89-112.

Henry-Gambier, D., Nespoulet, R., Chiotti, L., 2013. An Early Gravettian cultural attribution for the human fossils from the Cro-Magnon rock shelter (Les Eyzies-de-Tayac, Dordogne). Paleo 24, 121–138.

Holliday, T.W., 1997a. Body proportions in Late Pleistocene Europe and modern human origins. J. Hum. Evol. 32, 423-447.

Holliday, T.W., 1997b. Postcranial evidence of cold adaptation in European Neandertals. Am. J. Phys. Anthropol. 104, 245-258.

Holliday, T.W., 1999. Brachial and crural indices of European Late Upper Paleolithic and Mesolithic humans. J. Hum. Evol. 36, 549-566. https://doi.10.1016/j.jhevol.1998.0289.

Holt, B., 1999. Biomechanical Evidence for Decreased Mobility in Upper Paleolithic and Mesolithic Europe. Ph.D. Thesis, University of Missouri-Columbia.

Lartet, L., 1868. Une sépulture des troglodytes du Périgord (crânes des Eyzies). Bull. Soc. Anthropol. Paris 3, 335–349. https://doi.org/10.3406/bmsap.1868.9547.

Movius, H.L. Jr., 1969. The abri of Cro-Magnon, Les Eyzies (Dordogne) and the probable age of the contained burials on the basis of the evidence of the nearby Abri Pataud. Anuario de Estudios Atlanticos 15, 323-344.

Mussini, C., 2011. Les rested humains moustériens des Pradelles (Marillac-le-Franc, Charente, France): Étude morphométrique et réflexions sur un aspect comportemental des Néandertaliens. Thèse de Doctorat, Université de Bordeaux 1.

Nagurka, M.L., Hayes, W.C., 1980. An interactive graphics package for calculating cross-sectional properties of complex shapes. J. Biomech. 13, 59-64.

NCSS, 2016. NCSS 11 Statistical Software. NCSS, LLC., Kaysville, Utah; ncss.com/software/ncss.

Partiot, C., Trinkaus, E., Knüsel, C.J., Villotte, S., 2020. The Cro-Magnon babies: Morphology and mortuary implications of the Cro-Magnon immature remains. J. Archaeol. Sci. Rep. 30, 102257. https://doi.org/10.1016/j.jasrep.2020.102257.

Pruner-Bey, F., 1868. An account of the human bones found in the cave of Cro-Magnon, in Dordogne, in: Lartet, E., Christy, H. (Eds.), Reliquiae Aquitanicae: Being Contributions to Archaeology and Palaeontology of Périgord and the Adjoining Provinces of Southern France (1865-75). Williams and Norgate, London, pp. 73–92.

Puymerail, L., Volpato, V., Debénath, A., Mazurier, A., Tournepiche, J.F., Macchiarelli, R., 2012. A Neanderthal partial femoral diaphysis from the "grotte de la Tour", La Chaise-de-Vouthon (Charente, France): Outer morphology and endostructural organization. C. R. Palevol 11(8), 581-593. https://doi.org/10.1016/j.crpv.2012.07.001.

Rodríguez, L., Carretero, J.M., García-González, R., Arsuaga, J.L., 2018. Cross-sectional properties of the lower limb long bones in the Middle Pleistocene Sima de los Huesos sample (Sierra de Atapuerca, Spain). J. Hum. Evol. 117, 1-12. https://doi.org/10.1016/j.jhevol.2017.11.007.

Rohlf, F. J. (1998). TpsDig2. Ecology and Evolution, University of Stony Brook.

Ruff, C.B., 2019. Biomechanical analyses of archeological human skeletons. in: Katzenberg, M.A., Grauer, A.L. (Eds.). Biological Anthropology of the human skeleton, 3rd Ed. John Wiley and Sons, New York, pp. 189-224.

Ruff, C.B., Trinkaus, E.,Holliday, T.W. (2002) Body proportions and size. in: Zilhão, J., Trinkaus, E. (Eds.), Portrait of the Artist as a Child. The Gravettian Human Skeleton from the Abrigo do Lagar Velho and its Archeological Context. Trabalhos de Arqueologia 22, 365-391.

Ruff, C.B., Holt, B., Niskanen, M., Sládek, V., Berner, M., Garofalo, E., Garvin, H.M., Hora, M., Junno, J.A., Shuplerova, E., Vilkama, R., Whittey, E., 2015. Gradual decline in mobility with the adoption of food production in Europe. Proc. Natl. Acad. Sci. USA 112, 7147-7152. https://doi.10.1073/pnas.1502932112.

Ruff, C.B., Burgess, M.L., Squyres, N., Junno, J.A., Trinkaus, E., 2018. Lower limb articular scaling and body mass estimation in Pliocene and Pleistocene humans. J. Hum. Evol. 115, 85-111. https://doi.10.1016/j.jhevol.2017.10.014.

Schultz, M., Nováček, J., 2005. Vorläufige Ergebnisse paläopathologischer Untersuchungen an den postcranialen Skelettresten des paläolithischen Menschen von Brno II. Anthropologie (Brno) 43, 305-313.

Shackelford, L.L., 2007. Regional variation in the postcranial robusticity of Late Upper Paleolithic humans. Am. J. Phys. Anthropol. 133, 655–668. https://doi.10.1002/ajpa.20567.

Shang, H., Trinkaus, E., 2010. The Early Modern Human from Tianyuan Cave, China. Texas A&M University Press, College Station TX.

Slice, D. E., 2005. Modern Morphometrics in Physical Anthropology. New York, Plenum Press.

Sparacello, V.S., Villotte, S., Shaw, C.N., Fontana, F., Mottes, E., Starnini, E., Dalmeri, G., Marchi, D., 2018. Changing mobility patterns at the Pleistocene-Holocene transition: the biomechanics of the lower limb of Italian Gravettian and Mesolithic individuals. in: Cristiani, E., Borgia, V. (Eds.), Palaeolithic Italy: Advanced studies on early human adaptations in the Apennine Peninsula. Sidestone Press, Leiden. ISBN: 9789088905834. p. 357-396.

Stringer, C.B., Trinkaus, E., Roberts, M.B., Parfitt, S.A., Macphail, R.I., 1998. The Middle Pleistocene human tibia from Boxgrove. J. Hum. Evol. 34, 509-547. https://doi.org/10.1006/jhev.1998.0215.

Stock, J.T., Pfeiffer, S.K., Chazan, M., Janetski, J., 2005. F-81 skeleton from Wadi Mataha, Jordan, and its bearing on human variability in the Epipaleolithic of the Levant. Am. J. Phys. Anthropol. 128, 453-465. https://doi.10.1002/ajpa.20163.

Tardieu, C., Trinkaus, E., 1994. The early ontogeny of the human femoral bicondylar angle. Am. J. Phys. Anthropol. 95, 183-195. https://doi.10.1002/ajpa.1330950206.

Thibeault, A., Villotte, S., 2018. Disentangling Cro-Magnon: A multiproxy approach to reassociate lower limb skeletal remains and to determine the biological profiles of the adult individuals. J. Archaeol. Sci. Rep. 21, 76-86. https://doi.org/10.1016/j.jasrep.2018.06.038.

Thillaud, P.L., 1981. L'histiocytose X au Paléolithique (sujet no 1 de Cro-Magnon): problématique du diagnostic ostéo-archéologique. L'Anthropologie 85, 219–239.

Trinkaus, E., 1975. Squatting among the Neandertals: A problem in the behavioral interpretation of skeletal morphology. J. Archaeol. Sci. 2, 327-351. https://doi.org/10.1016/0305-4403(75)90005-9.

Trinkaus, E., 1981. Neanderthal limb proportions and cold adaptation. in: Stringer, C.B. (Ed.), Aspects of Human Evolution. Taylor & Francis, London. pp. 187-224.

Trinkaus, E., 2006. The lower limb remains. in: Trinkaus, E., Svoboda, J.A. (Eds.), Early Modern Human Evolution in Central Europe: The People of Dolní Věstonice and Pavlov. Oxford University Press, New York, pp.380-418.

Trinkaus, E., 2007. European early modern humans and the fate of the Neandertals. Proc. Natl. Acad. Sci. USA 104, 7367-7372. http://doi.10.1073/pnas.0702214104.

Trinkaus, E., 2018. An abundance of developmental anomalies and abnormalities in Pleistocene people. Proc. Natl. Acad. Sci. USA 115, 11941-11946. https://doi.10.1073/pnas.1814989115; PMID 30397116.

Trinkaus, E., Ruff, C.B., 1999. Diaphyseal cross-sectional geometry of Near Eastern Middle Paleolithic humans: The femur. J. Archaeol. Sci. 26, 409-424. https://doi 10.1006/jasc.1998.0343.

Trinkaus, E., Ruff, C.B., 2012. Femoral and tibial diaphyseal cross-sectional geometry in Pleistocene *Homo*. PaleoAnthropology 2012, 13-62. doi 10.4207/PA.2012.ART69.

Trinkaus, E., Zilhão, J., 2002. Phylogenetic implications. in: Zilhão, J., Trinkaus, E. (Eds.), Portrait of the Artist as a Child. The Gravettian Human Skeleton from the Abrigo do Lagar Velho and its Archeological Context. Trabalhos de Arqueologia 22, 497-518.

Trinkaus, E., Hillson, S.W., Franciscus, R.G., Holliday, T.W., 2006. Skeletal and dental paleopathology. in: Trinkaus, E., Svoboda, J.A. (Eds.), Early Modern Human Evolution in Central Europe: The People of Dolní Věstonice and Pavlov. Oxford University Press, New York, pp. 419-458.

Trinkaus, E., Buzhilova, A.P., Mednikova, M.B., Dobrovolskaya, M.V., 2014. The People of Sunghir: Burials, Bodies and Behavior in the Earlier Upper Paleolithic. Oxford University Press, New York.

Trinkaus, E., Lacy, S.A., Thibeault, A., Villotte, S., 2021a. Disentangling Cro-Magnon: The dental and alveolar remains. J. Archaeol. Sci. Rep. 37, 102991. http://doi.org/10.1016/j.jasrep.2021.102911.

Trinkaus, E., Thibeault, A., Villotte, S., 2021b. Disentangling Cro-Magnon: The pedal remains. Journal of Archaeological Science: Reports 40, 103228. https://doi.org/10.1016/j.jasrep.2021.103228.

Vallois, H.V., Billy, G., 1965. Nouvelles recherches sur les hommes fossiles de l'abri de Cro-Magnon. L'Anthropol. 69, 47–74.

Villotte, S., Balzeau, A., 2018. Que reste-t-il des hommes de Cro-Magnon 150 ans après leur découverte? Bull. Soc. Anthropol. Paris 30, 146–152. https://doi.org/10.3166/bmsap-2018-0026.

Villotte, S., Samsel, M., Sparacello, V.S., 2017. The paleobiology of the two adult skeletons from Baousso da Torre (Bausu da Ture) (Liguria, Italy): implications for our understanding of Gravettian lifestyle. C. R. Palevol 16, 462-473. https://doi.org/10.1016/j.crpv.2016.09.004.

Villotte, S., Thibeault, A., Sparacello, V., Trinkaus, E., 2020. Disentangling Cro-Magnon: The adult upper limb skeleton. J. Archaeol. Sci. Rep.33, 102475. https://doi.org/10.1016/j.jasrep.2020.102475.

Wu, X.J., Schepartz, L.A., Liu, W., Trinkaus, E., 2011. Antemortem trauma and survival in the Late Middle Pleistocene human cranium from Maba, south China. Proc. Natl. Acad. Sci. USA 108, 19558-19562. https://doi.10.1073/pnas.1117113108

Xing, S., Wu, X.J., Liu, W., Pei, S.W., Cai, Y.J., Tong, H.W., Trinkaus, E., 2020. Middle Pleistocene human femoral diaphyses from Hualongdong, Anhui Province, China. Am. J. Phys. Anthropol. 2020, e24121. https://doi.org/10.1002/ajpa.24121.

Zelditch, M. L., Swiderski, D. L., Sheets, H. D., & Fink, W. L., 2004. Geometric Morphometrics for Biologists: A Primer. Elsevier Academic Press, San Diego.

Describing Cro-Magnon: The Femora, Tibiae and Fibulae
Supporting Information

Erik Trinkaus, Vitale S. Sparacello, Song Xing, Adrien Thibeault, and Sébastien Villotte

1. Supporting Information Introduction

The lower limb long bones from the Cro-Magnon consist of portions of eight femora, four tibiae, and two fibulae [Cro-Magnon (CM) 4321 to CM 4335]. No patellae were recovered. The bones vary in completeness from a complete tibia (CM 4330) and a nearly complete fibula (CM 4334) to a partial femoral head and neck (CM 4321) and a small section of femoral diaphysis (CM 4323).

In the recent attempt to associate Cro-Magnon remains by individuals (Thibeault and Villotte, 2018), these remains (plus pelvic and two pedal bones) were assigned to three individuals, referred to as Alpha, Beta and Gamma (Table S1) [a fourth postcranial individual (Delta) is evident in the arm bones, and four individuals are represented in the craniofacial remains (Vallois and Billy, 1965; Villotte et al., 2020; Trinkaus et al., 2021a)]. Greek letter names were employed to avoid confusion with the four numbered craniofacial individuals, because the associations of these postcranial sets with the craniofacially represented individuals are largely unclear (see Trinkaus et al., 2021a). The only secure association of one of these postcranial sets is between Alpha and Cro-Magnon 1, based largely on shared pathological lesions and apparently similar ages-at-death. For these reasons, the remains discussed here are referred to by their Musée de l'Homme catalog numbers for individual elements and by Alpha to Gamma for the associated remains. [For a virtual articulation of the more complete Gamma lower limb remains, see: https://www.youtube.com/watch?v=L-HnxbMdP08].

The individual elements are presented here in terms of preservation, morphology and pathological lesions, following the descriptions of the upper limb and pedal remains (Villotte et al., 2020; Trinkaus et al., 2021b). Their comparative morphology is presented in the text. Given the presentations of the lower limb associations by individuals in Thibeault and Villotte (2018), it is only summarized here (Table S1; see Thibeault and Villotte, 2018: Table 4, Fig. 11).

The presentations of the Cro-Magnon femoral, tibial and fibular remains follow their attributions to postcranial individuals Alpha to Gamma, as opposed to sequential catalog numbers.

Table S1. Associations by individual of the Cro-Magnon femora, tibiae and fibulae.

	Alpha	***Beta***	***Gamma***
Femur – right	CM 4327	CM 4321	CM 4323, 4328
Femur – left	CM 4325	CM 4324, 4329	CM 4322
Tibia – right	CM 4332		CM 4333
Tibia – left	CM 4331		CM 4330
Fibula - right	CM 4335		CM 4334

2. The Cro-Magnon Femoral Remains

2.1. The Cro-Magnon femora

The eight preserved femoral elements from Cro-Magnon consist of one partial proximal epiphysis (CM 4321), a diaphysis with a partial proximal epiphysis (CM 4322), four variably complete diaphyses (CM 4323, 4324, 4325 and 4327), and two distal epiphyses with adjacent diaphyses (CM 4328 and 4329). In the original 19th century museum catalog (Fig. S1A), an additional left femoral diaphysis is listed (CM 4326); its whereabouts is unknown, and it does not appear in a late 19th century photograph of the Cro-Magnon femoral remains (Lainé, 1895).

In addition, there has been confusion over the numbering of one largely complete right femoral diaphysis. It was originally labeled on the medial diaphysis as "4323" (or "4323-1868-17" (Fig. S1B), which duplicated the number for the CM 4323 proximal right diaphysis. That number was subsequently edited on the bone with the addition of a "7," and more recently "4327" was written on the anteromedial neck (Fig. S1C). As a result, the bone has been referred to as "4327" (Vallois and Billy, 1965), "4323B" (Trinkaus and Ruff, 2012), and "4323/4327" (Thibeault and Villotte, 2018). From the original catalog, it is evident that the bone is Cro-Magnon 4327, a "diaphyse de fémur droit" (Fig. S1A). It will therefore be referred to as CM 4327. CM 4323 refers only to a short proximal diaphyseal section.

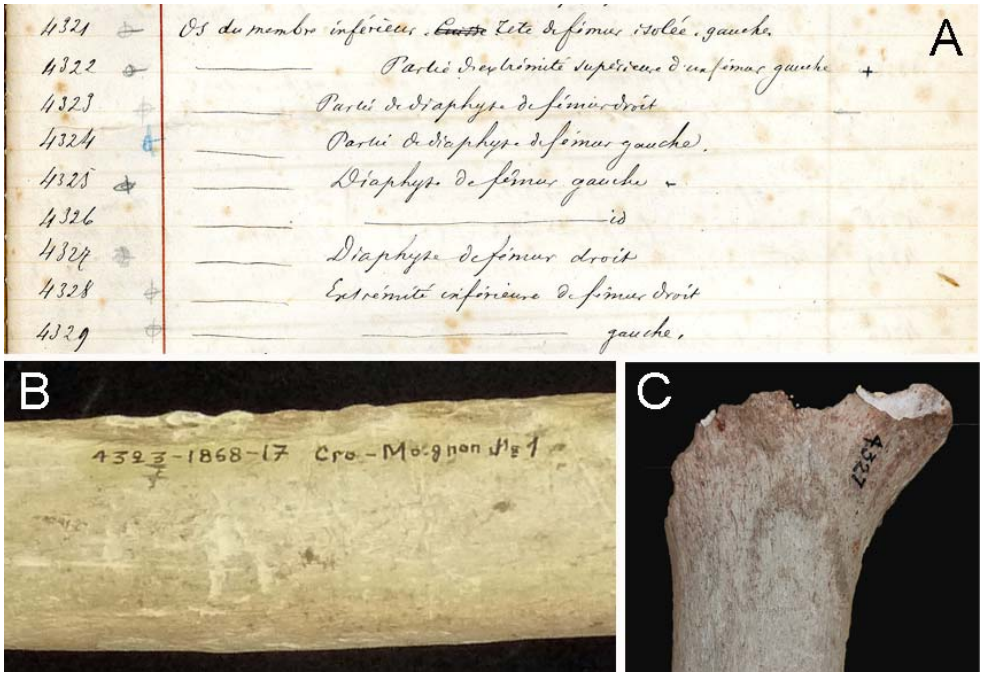

Figure S1. A: The femoral portion of the original Musée de l'Homme catalog entry, with 4323 labeled as "Partie de diaphyse de fémur droit" and 4327 labeled as "Diaphyse de fémur droit." B: The original notation on the medial midshaft, with the full catalog number (4323-1868-17) and "Cro-Magnon No. 1", amended with a "7" below the "3" of 4323. C: A more recent 4327 number added to the anteromedial base of the neck. Given the completeness of this diaphysis and only proximal diaphyseal preservation of the CM 4323 femur (Fig. S2), it is apparent that the more complete femoral diaphysis is CM 4327, was mislabeled originally, and then subsequently amended.

Figure S2. The Cro-Magnon femora in anterior view. The four to the left (4325, 4322, 4324 and 4329) are left; the other three are right. The diaphyseal pieces are aligned with respect to their gluteal tuberosities.

Figure S3. The Cro-Magnon femora in posterior view, arranged and aligned as in Fig. S2.

Figure S4. The Cro-Magnon femora in medial view, arranged and aligned as in Fig. S2.

Figure S5. The Cro-Magnon femora in lateral view, arranged and aligned as in Fig. S2.

2.2 Femur Right 4327 (Alpha)

2.2.1 Preservation

The bone retains the diaphysis from the start of the medial curvature of the neck to a few centimeters above the emergence of the epicondyles. The greater and lesser trochanters are missing and for the proximal portion of the bone, only the medial and anterior surfaces are present. The beginning of the supracondylar roughness is evident posteriorly on the distal margin.

2.2.2 Morphology

The diaphysis appears to exceptionally massive for its length (see strength assessment in the text). The appearance of hypertrophy is emphasized by the large pilaster, which is further emphasized by bony protrusions along the linea aspera (Figs. S3, S9 and S10).

Figure S6. Posteromedial views of the Alpha femora (CM 4327 right femur and CM 4325 left femur), with the spiral lines and the pectineal crests. The broken distal margins of the lesser trochanters are above. Scale bar: 5 cm.

Proximally there appears to have been strong anteversion of the head and neck, as indicated by the preserved portion of inferomedial neck relative to the parasagittal plane through the linea aspera. The preserved neck portion also indicates a high neck-shaft angle, at least as high as the ≈129° angle of CM 4322 (Fig. S19; Table S5), which places it among the E/MUP femora with the highest angles (see Fig. 5).

Insufficient portions of trochanters are preserved to indicate their morphology, but the spiral line (for vastus medialis) is strongly marked (Fig. S6). It is notably irregular, with localized enthesophytes projecting medially. It runs all along the posterior, medial and anterior surfaces. Anteriorly, the line seems to form a "C," with the concavity facing distally and the convexity proximal.

In the subtrochanteric region, there is a clearly marked lateral gluteal buttress, extending obliquely from a more anterior position proximally to a more posterior position distally (Figs. S3, S4 and S7). It is ≈74 mm proximodistally and up to 14 mm thick anteroposteriorly. There is a flat to modestly concave area anteriorly, accentuating the projection of the buttress (Fig. S7). A relatively well marked subtrochanteric sulcus or fossa is present posteriorly, the floor of which is visually irregular but relatively smooth when palpated (Fig. S8) The pectineal line is visible, raised and irregular (Figs. S6 and S8).

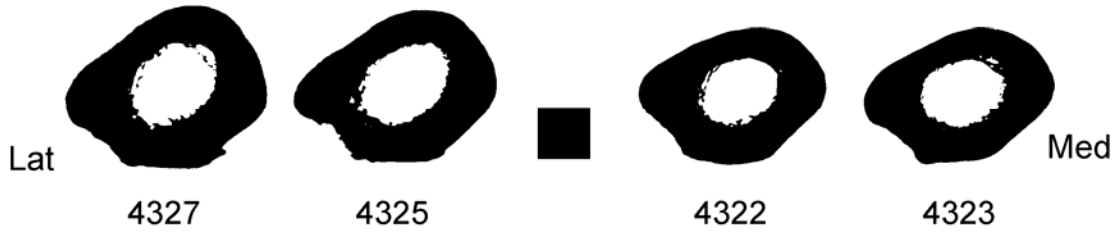

Figure S7. Subtrochanteric (80%) cross-sections of the Cro-Magnon femora. Anterior is above. The CM 4325 and 4322 left femora are as viewed from proximal; the right CM 4327 and 4323 sections are reversed so that lateral is on the left for all four sections. The scale is 1 cm square.

Figure S8. Posterolateral views of the CM 4327 (right) and CM 4325 (left) (Alpha femora) subtrochanteric regions, showing their gluteal tuberosities. Scale bar: 5 cm. The probabaly age-related bony growths (the purported "incipient" third trochanters) are indicated by arrows.

The gluteal tuberosity is broad (Table S2; Fig. S8), and the gluteal line is irregular and rough, sharp and prominent. Given the smooth nature of the gluteal tuberosity, the even curve from the sulcus to the lateral gluteal buttress, and the absence of a distinct depression (or fossa) proximally in the sulcus, the femur lacks a hypotrochanteric fossa (*sensu* Houzé, 1883; Hrdlička, 1934; *contra* Vallois and Billy, 1965).

In their discussion of the Cro-Magnon femora, Vallois and Billy (1965: 259) noted that one of them presents an incipient third trochanter. Both CM 4327 and 4325 preserve the area (none of the other Cro-Magnon femora preserve the relevant portion), and each exhibits a small rugose swelling. It is unclear whether these rugosities represent "incipient" or "slight" third trochanters, but they are unlike the prominent knobs normally categorized as third trochanters (Hrdlička, 1937; Bolanowski et al., 2005) and present on about half of the E/MUP femora (Trinkaus et al., 2014). It is most likely that these small protuberances represent age-related growths of the proximal gluteal tuberosity muscle insertion rather than any discrete trait of the region.

There is a distinct anterior convexity to the CM 4327 diaphysis, which is evident primarily in the mid-proximal diaphysis, slightly distal of the gluteal tuberosity (as noted by Pruner-Bey, 1868; Figs. S4 and S5). The more distal two-thirds of the shaft have little anterior convexity. A similar pattern is evident in its antimere (CM 4325) but not in the CM 4322 Gamma femur.

There is a clearly demarcated medial buttress (≈70 mm long and ≈14 mm thick), showing up as a distinct swelling along the proximal half of the diaphysis (see Trinkaus, 1976). It rotates around the medial shaft from slightly anterior proximally to slightly posterior at its distal extent, and it is particularly evident in the subtrochanteric region (Fig. S6).

As noted above, the pilaster is massive and extremely well marked (Fig. S9). It has a strong longitudinal sulcus laterally, but medially it is anteroposteriorly flat. Interestingly, early descriptions of the Cro-Magnon femora (Broca, 1868; Pruner-Bey, 1868) emphasized the large size of the CM 4327 pilaster, although Pruner-Bey (1868) noted the much smaller pilasters on CM 4322 and 4324. Even Vallois and Billy (1965), despite providing a midshaft cross-section of CM 4322 and pilastric indices for all four Cro-Magnon femora midshafts, discussed only the large one on CM 4327.

The linea aspera is irregular with substantial bony projections (see below). The lateral supracondylar ridge is not especially evident, and the medial one is neither visible nor palpable.

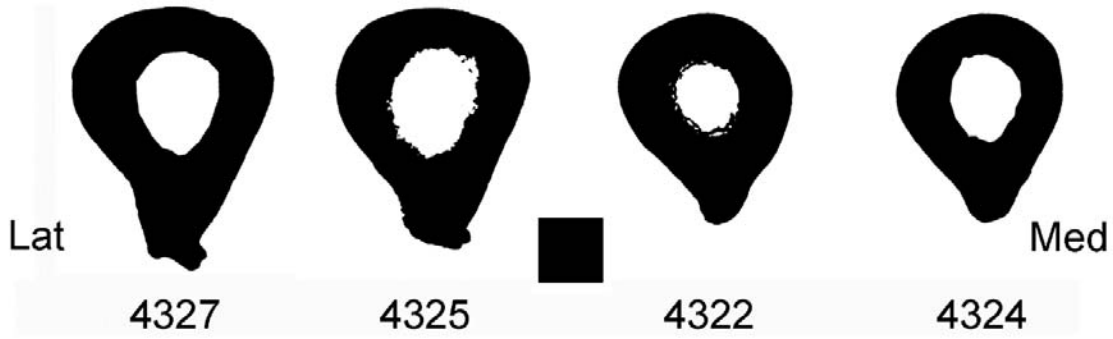

Figure S9. Midshaft (50%) cross-sections of the Cro-Magnon femora. Anterior is above. The CM 4325, 4322 and 4234 left femora are as viewed from proximal; the right CM 4327 section is reversed so that lateral is on the left for all four sections. The scale is 1 cm square.

2.2.3 Paleopathology

The CM 4327 femur exhibits bony growths along its spiral line and linea aspera. The spiral line is generally strongly marked (Fig. S6), but there is also a bony projection ≈16 mm long extending anteromedially at the level of the distal lesser trochanter (Fig. S10). This growth is accompanied by large bony projections 4 to 6 mm wide along the linea aspera through midshaft (Figs. S4, S9 and S10). These bony projections are discontinuous. The discontinuities seem to be related at least in part to the passage of veins or arteries, given various venous imprints along the shaft. There is also bony growth forming a small and more regular crest on the lateral lip of the linea aspera.

Figure S10. Bony projections on the CM 4327 femur. Left: Anteromedial view of the spiral line with the bony knob indicated. Right: posteromedial view of the mid-linea aspera with the medially directed bony projections highlighted by shadows. Scale bar: 5 cm.

The bony growth on the lateral linea aspera, along with those in the subtrochanteric area, appear as common bony growth along muscle attachments, especially in older individuals. The bony growth in the middle of the spiral line and along the medial linea aspera are more pronounced, and they should both be related to the attachments of the vastus medialis muscle.

2.3 Femur Left 4325 (Alpha)

2.3.1 Preservation

The bone retains the diaphysis from the distal end of the curvature of the neck at the proximal end of the lesser trochanter to a few centimeters above the emergence of the epicondyles. The greater and lesser trochanters are absent, although the distal swelling for the lesser trochanter is preserved. Primarily proximally the medial and anterior surfaces are present.

2.3.2 Morphology

The bone is massive, but it appears to be less robust than its antimere, CM 4327 (see text). There is a strong anterior convexity to the midproximal diaphysis, similar to the one on CM 4327 (see also Pruner-Bey, 1868). Although it cannot be measured, the orientation of the preserved inferolateral neck suggests a well-developed head and neck anteversion.

There is a strong and clearly demarked gluteal buttress, oblique from a more anterior position proximally to a more posterior position distally (Figs. S7 and S8). It extends for ≈70 mm and is maximally ≈10 mm thick. There is a flat area with slight concavity anteriorly that accentuates the buttress, and there is a relatively well marked subtrochanteric fossa posteriorly, similar to CM 4327. The floor of the fossa is irregular, delineating a clear gluteal tuberosity, but it is relatively smooth when palpated; it is more of a longitudinal sulcus rather than a discrete fossa. At the proximal end of the sulcus there is a small swelling of bone (Fig. S8), which could be considered to be an incipient third trochanter but is insufficient to be scored as such (see above).

The spiral line runs all along the posterior and medial surfaces, with a moderately broad rugosity, but it is visible and palpable anteriorly (Fig. S6). Despite its rugosity, it lacks the small tubercles of bone present on the CM 4327 spiral line.

There is a clearly demarcated medial buttress, especially proximally, similar to the one on the right side. The pilaster is strongly built and well delineated by a lateral longitudinal sulcus and a flat medial side (Figs. S3 and S9). Yet, it is less prominent than the right one. The lateral supracondylar ridge is visible, and the medial one is only partly apparent.

2.3.3 Paleopathology

The gluteal tuberosity is irregular and rough, and its medial margin is created by a strong gluteal line (Fig. S8). The spiral line presents small enthesophytes projecting medially, at the level of the distal lesser trochanter. As noted, it lacks the large bony projections present on its antimere.

The linea aspera is irregular with bony projections of 2 to 4 mm through the midshaft, from its medial border projecting medially (Fig. S11). This bone projection is not as discontinuous as on the right side, although there are similar and variable venous imprints along both shafts. There is also bone forming a small crest on the lateral lip of the linea aspera, but those growths are fewer and less projecting.

Figure S11. Posteromedial view of the CM 4325 femoral midshaft, showing the medial lip of bone along the linea aspera. Scale bar: 5 cm.

At the border between the anterior and lateral surfaces of the shaft, 44 mm from the distal break, there is a large lesion (Fig. S12). This lesion was first noted by Broca (1868) and Pruner-Bey (1868). The former considered it to be entirely traumatic in origin, and he used it to reinforce ideas concerning the violent nature of Pleistocene humans (see comments by Dastugue, 1967). Pruner-Bey was less certain of its etiology, and he attributed it to either trauma or a localized inflammation ("caries"). More recently Dastugue (1967) interpreted the lesion as secondary to adjacent soft tissue abnormalities, and he considered it to be part of a systemic condition also involving lesions on the cranium, mandible and left ilium (see Fig. 13). The abnormality is merely described here; no diagnosis is presented.

For description, the lesion is considered to be on the lateral surface, although it rounds onto the anterior diaphysis. The total affected area is ≈56 mm proximodistal and ≈30 mm anteroposterior. The outer limits are not well circumscribed. The primary area of the lesion

corresponds roughly to an ovoid area of raised cortical bone with microporosity on the anterior versant (providing possible evidence of hypervascularisation). The proximal area resembles a triangular comet tail shape. The posterior border is less distinct and does not seems to be raised relative to the adjacent subperiosteal bone. The overall structure is irregular but smooth.

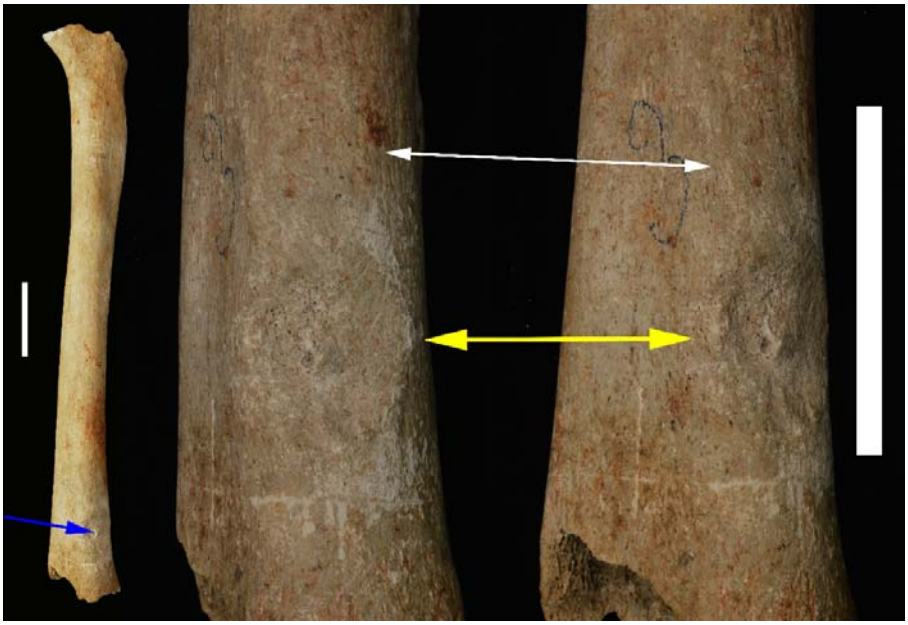

Figure S12. Left: anterior view of the CM 4325 left femur, with the location of the distal diaphyseal lesion indicated (blue arrow). Lateral (middle) and anterolateral (right) detailed views of the CM 4325 distal femoral lesion. The primary lesion is indicated by the yellow arrow. A less pronounced area proximal of the primary lesion is indicated by the white arrow. Scale bars: 5 cm. See also Fig. 16.

Figure S13. Lesions on the right frontal bone of CM 4253 (Cro-Magnon 1) and the anterosuperior external left ilium of CM 4314b (Alpha), referred to a systemic condition by Dastugue (1967). Additional lesions are present on the heads of the CM 4347 and 4349 metatarsals and the CM 4351 hallucal phalanx (Trinkaus et al., 2021b). The left mandibular lesion, considered to be part of the Cro-Magnon 1 systemic syndrome by Dastugue (1967), is more likely due to periodontal disease and granulomata (Trinkaus et al., 2021a).

Inside this elevated area, there is a relatively well circumscribed depression, approximately circular and ≈21 mm in diameter. The surface of the posterior half is similar to normal cortical bone; the anterior half displays microporosity. Close to the posterior half, there is a raised area associated with a deep circular pit, which nonetheless does not perforate the cortical bone.

2.4 Femur Right 4321 (Beta)

2.4.1 Preservation

The piece consists of the head and partial neck of a right femur, from the fovea capitis to the lateral two-thirds of the neck (Fig. S14). The head is largely intact, but there is a large area superoanteriorly (≈30 mm by ≈12 mm) along the articular margin where the articular surface is absent and trabeculae are exposed. The neck is preserved for ≈20 to 25 mm from the margin of the head, especially posteriorly, such that a large part of the anterior surface of the neck (≈25 by ≈25 mm) is missing, especially laterally. The articular surface, where present, is well preserved except for some small patches of abrasion. The inferior margin is missing a section ≈15 mm long and up to 5 mm wide.

CM 4321 is the only femoral head from Cro-Magnon which is sufficiently intact to provide a diameter directly. The other femoral head diameters (Table S4) are reconstructed (CM 4322) or estimated from associated acetabula.

Figure S14. Posterior (left) and anteroproximal (right) views of the CM 4321 right femoral head and adjacent partial neck. Scale bar: 5 cm.

2.4.2 Morphology

The head articular surface is featureless. The teres ligament attachment (fovea capitis) is smooth, with microporosity present in an area ≈5 mm in diameter.

The neck displays a sulcus on its superoposterior surface; it is a slightly depressed area, without any articular indications. Its clear margin is preserved medially and inferiorly. It is well circumscribed inferiorly but the margin faints away in the superior portion of the medial border of the facet. Superiorly, for the part of the neck preserved, the margin is not clearly visible.

Posteriorly, below the sulcus, the neck displays a foramen close to the head-neck junction, which is followed by a transverse sulcus that looks like a vascular imprint. Although the anterior head-neck region is largely absent, there is no evidence of either a Poirier's facet or an Allen's fossa.

2.4.3 Paleopathology

Although the head articular surface is normal, there is a minor osteophytic swelling (1 to 2 mm wide) along its margin inferiorly and posteriorly.

2.5 Femur Left 4324 (Beta)

2.5.1 Preservation

The partial CM 4324 diaphysis retains 230 mm laterally from the proximal gluteal tuberosity to the mid-distal shaft. Medially it is present from the level of distal end of the gluteal buttress to roughly midshaft. The proximal break is oblique from proximolateral to distomedial. The distal break is oblique from proximomedial to distolateral. This pattern makes the shaft far more present laterally than medially. The minimum medial length is only 82 mm.

There are two reconstructed breaks, one approximately at midshaft and the other oblique in the distal portion; the pieces fit well with no distortion. The cortical bone is longitudinally abraded on the preserved medial surface. There have been several analytical samples taken from the internal cortical bone at the proximal break.

The CM 4324 left diaphysis is very likely a portion of the same bone as the CM 4329 distal left femur (Thibeault and Villotte, 2018). Aligning the two elements, however, indicates that there is no contact between them (Fig. S4). The two pieces together therefore provide a minimum length from the distal condyles to the proximal gluteal tuberosity for the Beta left femur.

Figure S15. Proximal posterior view of the CM 4324 left femur, with the proximal end of the linea aspera, the gluteal tuberosity and the pectineal crest. Scale bar: 5 cm.

2.5.2 Morphology

The bone has a well-marked gluteal buttress (≈70 mm long) with a shallow depression anteriorly and a marked sulcus posteriorly (Figs. S3 and S15). The posterior sulcus is the floor of the gluteal tuberosity, accentuating it and creating a relatively well marked subtrochanteric fossa posteriorly. The floor of the anterior depression and the gluteal line are irregular but

relatively smooth, not especially sharp or prominent. The spiral line is slightly irregular and there is no clear trace of the pectineal line.

The gluteal tuberosity is strongly marked, with irregular but smoothed swellings and fossae within the sulcus, especially proximally (Fig. S15). The linea aspera is regular, with a breadth near midshaft of 7.2 mm and one of 7.8 mm near its proximal end. The pilaster is well formed, with an adjacent flat medial surface and a modest sulcus along it laterally. It lacks the prominence evident in the CM 4325 and 4327 femora. The shaft gives the impression of being relatively convex anteriorly (Fig. S4), but that is likely due its incomplete nature. However, it is especially concave laterally (Fig. S2).

2.5.3 Paleopathology

There are no abnormalities evident on the partial diaphysis.

2.6 Femur Left 4329 (Beta)

2.6.1 Preservation

The bone retains its distal third. The proximal break is oblique, from proximoanterior to distoposterior. The medial surface proximal of the medial epicondyle is broken away over an ovoid area 30 mm proximodistal by 40 anteroposterior (Fig. S16). Both condyles have the medial and lateral margins of their articular surfaces abraded, the main areas being the medial margin of the medial condyle and the lateral margin of the lateral one. There are two patches of loss of articular subchondral bone (9.5 by 7.0 mm for one, 6.5 mm in diameter for the other one) on the distal surface of the medial condyle (Fig. S16).

There is a hole in the medial surface of the shaft for sampling, which is 3 mm in diameter externally but resulted in a large removal of bone endosteally.

2.6.2 Morphology

The lateral supracondylar ridge is evident at the angular junction of the posterior and lateral surfaces of the shaft, but it is not raised. The medial one is neither visible nor palpable. The adductor tubercle is evident as a small, smooth elevation of bone.

The femoral condyles are evenly rounded. There is no evidence of femoral squatting facets, a flattening of the proximoposterior condylar articular bone (see Trinkaus, 1975). On lateral side, there is a smooth transverse sulcus separating the condylar surface from the patellar one; the medial sulcus is less clearly marked but present. The patellar surface is modestly larger on the lateral side, such that its lateral breadth is 57.9% of the patellar facet breadth.

2.6.3 Paleopathology

The margin of the patellar articular surface is slightly raised (a minor osteophytic border), especially on the proximomedial part (2 to 4 mm wide, 1 to 2 mm of protrusion).

Lateral of the adductor tubercle, ≈6 mm above the proximal limit of the medial condyle, there is a relatively well circumscribed, roughly circular, area of cortical excavation (Fig. S16). The floor is irregular with bony spicules. There is no elevation of bone around the lesion, and it is not associated with an elevation of the medial supracondylar ridge (which is not visible). It is a mild form of a bony reaction likely related to stress from the medial head of the gastrocnemius muscle (Resnick and Greenway, 1982).

Figure S16. Anterior (left) and posterior (right) views of the CM 4329 distal femur. The raised patellar surface margin is evident in the anterior view, and as is the medial condylar articular depressed area in the posterior view. The area of posteromedial supracondylar excavation, for the medial head of the gastrocnemius muscle, is indicated by the arrow in the posterior view. Scale bar: 5 cm.

The medial condyle displays on its distoposterior surface, 20 mm from its distal end, roughly midway between the lateral and medial margins, a small (2.6 mm diameter) depressed area with well circumscribed margins (apart from the anterior one). The floor of it is smooth, and the margins are not raised or irregular. There are no foramina. It is likely an inferocentral osteochondritis dissecans; it resembles the changes seen on the CM 4294 and 4295 distal humeri, also attributed to Beta (Villotte et al., 2020).

2.7 Femur Left 4322 (Gamma)

2.7.1 Preservation

The bone retains the complete shaft and the posterior half of the proximal extremity (Figs. S2 to S5). Only the central and posterior portions of the head are preserved, such that the articular surface is preserved only posteriorly (37 x 20 mm). None of the articular margins is preserved. The anterior and medial neck are absent, as well as the anterior and inferolateral portions of the greater trochanter. The lesser trochanter is missing, broken at its base. The distal end appears to be just proximal of the distal diaphyseal flare for the epicondyles.

There is a transverse break at the junction between the shaft and neck, through the base of the lesser trochanter. There is an oblique (proximolateral to distomedial) break across the distal third of the gluteal tuberosity, and the anterior piece and portions of the subtrochanteric area have been glued together. There is also a transverse break across the proximal popliteal surface, 60 mm above the distal end of the bone. All of these breaks were glued and missing edges filled with wax, without any apparent separation of the pieces.

As such it is the most complete of the Cro-Magnon femora, retaining most of the bone in continuity from the proximal head almost to the distal epiphysis. It has been possible to reconstruct the missing portions of the head, determining the radius of the head from the existing contour and then fitting the resultant sphere to the preserved portion (Thibeault and Villotte, 2018; Fig. S17). In addition, by mirror imaging the CM 4328 distal right femur and matching it to the CM 4322 distal diaphysis (Fig. S18), it is possible to provide a largely complete femur for Gamma, including highly reliable measures of bone lengths and its head diameter (Tables S2 and S4).

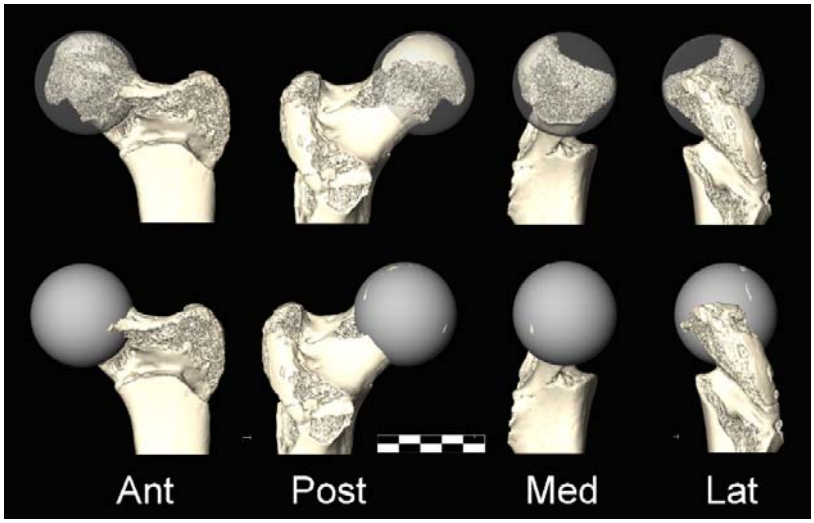

Figure S17. Virtual reconstruction of the femoral head of CM 4322 by determining the radius of curvature of the head from the preserved articular contour, and then fitting a sphere of that radius to the preserved head portion and proximal femoral neck. See Thibeault and Villotte (2018).

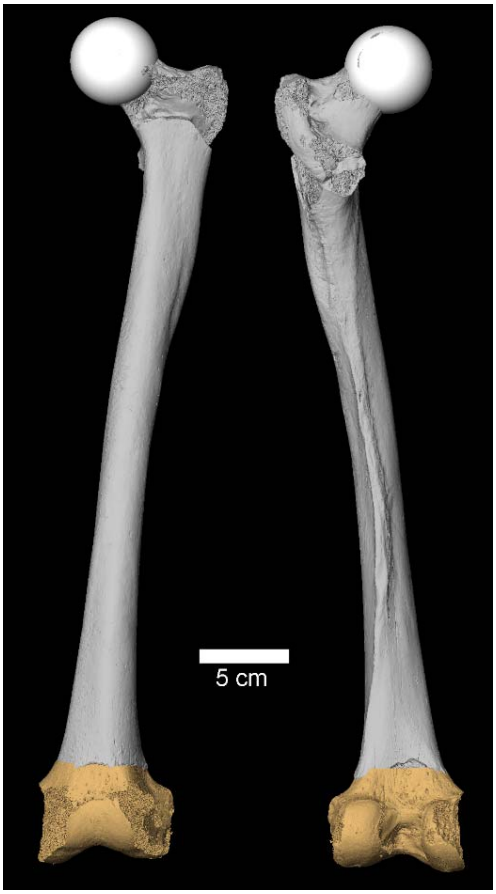

Figure S18. Anterior and posterior views of the CM 4322 left femur (gray), completed with the sphere for the femoral head (see Fig. S17) and the mirror imaged distal epiphysis of CM 4328 (beige).

2.7.2 Morphology

There is little of note on the preserved portions of the head and neck. The neck-shaft angle of ≈129° is relatively high for an earlier Upper Paleolithic femur (119.8° ± 5.7°, n =

21), exceeded only by the values for Dolní Věstonice 3 and Nahal Ein Gev 1 (Fig. 5). The value is approximate given the reattachment of the neck and greater trochanter to the proximal shaft (Fig. 19). However, Vallois and Billy (1965) provided the same value of ≈129°.

Figure S19. Posterior views of the CM 4322 and 4327 proximal femora. The CM 4322 femur illustrates its high neck-shaft angle. The preserved portion of the CM 4327 medial neck indicates a similar or higher neck-shaft angle.

There is a strong and clearly demarcated gluteal buttress, running obliquely from a more anterior position proximally to a more posterior position distally. It is ≈ 84 mm long and ≈13 mm thick. It is delimited by a slight depression anteriorly accentuating the buttress, and a relatively well marked subtrochanteric sulcus posteriorly. The floor of the sulcus is irregular and rough when palpated (Fig. S20). The gluteal line is irregular and rough, sharp but not extremely developed. The spiral line is prominent and slightly irregular (Fig. S20), for the vastus medialis origin. The surface bone between the base of the lesser trochanter and the spiral line is irregular, with wavy low relief lines (Fig. S20); the significance of these lines is unclear. The pectineal line is visible.

The pilaster is moderately prominent (far less than those of CM 4235 and especially CM 4327) and exhibits moderate longitudinal sulci medially and laterally (Figs. S3 and S9). The linea aspera is only slightly irregular and is not expanded transversely. The lateral supracondylar ridge is visible at the angle between the posterior and lateral surfaces of the shaft, and it forms a raised rounded crest. The medial ridge is neither visible nor palpable.

There is only a slight anterior diaphyseal curvature, and just a hint of the mid-proximal curvature evident on CM 4325 and especially CM 4327 (Fig. S5). There is no evidence of a medial buttress.

2.7.3 Paleopathology

The limited preserved portion of head articular surface displays no changes. The very small preserved area of attachment for the gluteus medius on the greater trochanter displays a tiny (3 x 1 mm) area of erosion; its origin is unclear. The attachment for the gluteus maximus fibers in the trochanteric fossa displays two spicules of bone (each projecting ≈2 mm), and the bases of three other ones that are broken (Fig. S20).

There are at least two small depressions in the middle of the anterior surface, approximately at the level of the proximal end of the gluteal fossa. It is in the same area as a depression on its antimere, CM 4323, but there are no foramina within the depressions and the margins are not raised. Their etiology is unclear, and they may not be pathological.

There are two venous imprints on the diaphysis, of uncertain significance. One imprint, 29 mm long, is on the medial surface, at the level of the proximal end of the distal third of the diaphysis, running obliquely from proximoposterior to distoanterior. The other one is a shorter but broader imprint (≈10mm long) just proximal of first one, oblique from proximoanterior to distoposterior. The second one in particular goes into the medial linea aspera.

Figure S20. The gluteal tuberosities of The CM 4322 and 4323 femora (left) and the spiral line of the CM 4322 left femur (right). Scale bar: 5 cm.

2.8 Femur Right 4323 (Gamma)

2.8.1 Preservation

The bone retains a portion of proximal diaphysis, corresponding roughly to the length of subtrochanteric fossa (Fig. S20). The distal portion was sawed transversely, such that a centimeter or two of irregular bone was removed. It is unclear when or for what purpose the bone was sawed; the original fossilization edge was present in the 1890s (Lainé, 1895), but it had been removed by 1980 (ET photos).

2.8.2 Morphology

There is a strong gluteal buttress (≈13 mm thick; its length cannot be measured because of proximal and distal breaks), oblique from a more anterior position proximally to a more posterior position distally. A slight depression anteriorly accentuates the buttress, and a relatively well marked subtrochanteric sulcus is present posteriorly. The floor of sulcus is clearly irregular and rough when palpated (Fig. S20). The gluteal line is irregular and rough, sharp but not extremely developed. The spiral line is well marked and slightly irregular, and the pectineal line is visible.

2.8.3 Paleopathology

There is a small depression (7 mm proximodistal, 5 mm mediolateral, but not well circumscribed) in the middle of the anterior surface, close to the proximal break. The margin

is slightly raised, and some small foramina are at its bottom. Its etiology is unclear, and it may not be strictly pathological.

2.9 Femur Right 4328 (Gamma)

2.9.1 Preservation

The bone retains its distal third, from proximal end of the lateral deviation of the linea aspera to the distal surfaces of the condyles. The medial third of the whole medial condyle (including the adductor tubercle) is missing. The lateral margin and the surface of the lateral epicondyle are heavily abraded. The remainder of the lateral condyle is well preserved, but the lateral portion of the medial condyle has small preservation defects. The patellar and distal condylar surfaces are well preserved.

The proximal break was cleanly transverse, at least as recently as 1980 (ET photo). Since then, 1 to 2 cm of the bone was removed from the proximal shaft, and a sample was drilled from the posterior cortical bone, for biomolecular analysis (Fu et al., 2013); the destructive sampling and analyses were undertaken, although it had already been demonstrated (Henry-Gambier, 2002) that the Cro-Magnon human remains lacked sufficient organic preservation for such analyses (once again, evidence of paleogeneticists operating in ignorance of the paleoanthropological literature).

2.9.2 Morphology

The lateral supracondylar ridge is visible at the angle between of the posterior and lateral surfaces of the shaft, and it forms a raised rounded crest. The medial ridge is neither visible nor palpable. There is no proximoposterior flattening of the lateral condyle [a femoral squatting facet (Trinkaus, 1975)]; the area for a medial one is not preserved.

2.9.3 Paleopathology

The posterior surface, just above the condyle, is rough but no clear tubercles or depressions are present. There is a slight osteophytic ridge on the preserved side for 8 mm of the anterior patellar surface margin, and slight osteophytes are along the posterior margin of the medial condyle, projecting less than 1 mm. There are smooth attachments for the cruciate ligaments.

2.10 Femoral Osteometrics and Cross-Sectional Geometry

Table S2. Osteometric dimensions of the femora: Lengths and diaphyses. In millimeters.

	M#	*Alpha Right*	*Alpha Left*	*Beta Left*	*Gamma Right*	*Gamma Left*
		4327	***4325***	***4324***	***4323***	***4322***
Maximum length[1]	1	(488.6)	(492.4)	(457.5)	--	477.0[2]
Bicondylar length[3]	2	(486.2)	(490.0)	(454.7)	--	475.5
Biomechanical length[4]		(462.1)	(465.6)	(433.0)	--	449.3
Midshaft sagittal diameter	6	40.4	37.2	31.4	--	32.0
Mid. transverse diameter	7	31.2	29.7	25.3	--	27.0
Midshaft circumference	8	114.0	107.0	89.0	--	92.0
Proximal sagittal diameter	10	31.6	29.6	--	25.4	25.7
Prox. transverse diameter	9	38.0	38.7	--	35.9	35.5
Proximal circumference		109.0	107.0	--	98.0	98.0
Gluteal tuber. breadth[5]		12.3	10.5	12.5	12.9	11.2
Hypotrochanteric fossa		absent[6]	absent[6]	absent[6]	absent[6]	(absent)
Third trochanter		absent[7]	absent[7]	--	--	--

[1] The maximum lengths of the CM 4327, 4325 and 4327 femora were estimated by matching surface renderings of the preserved portions of the femora to renderings of five Upper Paleolithic individuals (Thibeault and Villotte, 2018).

[2] The three lengths of the CM 4322 femur were determined from the virtual model of the CM 4322 left proximal and diaphyseal femur plus the mirrored CM 4328 right distal femur (Fig. S18; see also Fig. S17).

[3] The bicondylar lengths of the CM 4324, 4325 and 4327 femora were estimated from their maximum lengths using a regression based on recent humans (= 1.012 x FemMaxLen – 8.38, $r^2 = 0.996$, n = 40).

[4] The distance parallel to the diaphyseal axis, from the proximal neck just medial of the greater trochanter to the average of the distal condyles (Ruff and Hayes, 1983). The biomechanical lengths of the CM 4324, 4325 and 4327 femora were estimated from their maximum lengths using a regression based on Upper Paleolithic femora (= 0.934 x FemMaxLen + 5.5, $r^2 = 0.956$, n = 35).

[5] The mid-tuberosity breadth of the gluteal tuberosity.

[6] The gluteal tuberosity is transversely concave along its length but lacks a distinct ovoid depression in the proximal tuberosity.

[7] A small swelling is present at the proximal end of the gluteal tuberosity, which may represent an incipient third trochanter, but it cannot be categorized as present.

Table S3. Cross-sectional geometric properties of the Cro-Magnon femora at midshaft (at 50% of biomechanical length) and the subtrochanteric level (at 80% of biomechanical length). Areas in mm^2; second moments of area in mm^4; section moduli in mm^3.

	Alpha Right 4327	***Alpha Left 4325***	***Beta Left 4324***	***Gamma Right 4323***	***Gamma Left 4322***
Midshaft (50%)					
Total area	830.2	772.5	582.7		601.1
Cortical area	676.6	603.0	472.6		523.8
A-P 2nd moment of area (Ix)	75560	61204	33172		34471
M-L 2nd moment of area (Iy)	42343	36752	21609		24722
Max. 2nd moment of area (Imax)	75719	61338	33207		35540
Min. 2nd moment of area (Imin)	42183	36618	21573		23704
Polar moment of area (J,Ip)	117903	97956	54781		59244
A-P section modulus (Zx)[1]	3433	3025	1958		1996
M-L section modulus (Zy)[1]	2569	2346	1634		1748
Polar section modulus (Zp)[1]	5661	5047	3369		3494
Subtrochanteric (80%)					
Total area	863.9	803.5		679.0	685.3
Cortical area	669.7	608.1		521.8	541.0
A-P 2nd moment of area	46800	37817		25436	26930
M-L 2nd moment of area	70361	64497		49798	48733
Max. 2nd moment of area	72801	66074		51322	49451
Min. 2nd moment of area	44360	36239		23912	26212
Polar moment of area	117161	102313		75234	75663

[1] Section moduli computed from second moments of area and external diameters, following Trinkaus and Ruff (2012).

Table S4. Transverse head diameters (in mm) for the Cro-Magnon femora, from Thibeault and Villotte (2018), and body mass estimates (in kg) based on Ruff et al. (2018).

	Alpha Right	***Alpha Left***	***Beta Right***	***Gamma Right***	***Gamma Left***
			4321		***4322***
Head diameter: femur			42.2[1]		(49.4)[2]
	4314a	***4314b***	***4317***	***4318***	***4315***
Head diameter: coxal[3]	(46.7)	(48.6)	(42.9)	(49.8)	(50.0)
Body mass estimate[4]	69.1		56.8	73.0	

Notes to Table S4.

[1] The CM 4321 value is a direct measurement of the proximal femur.

[2] The CM 4322 estimate is from a virtual reconstruction of its femoral head, using the contour of the preserved portions of articular bone (Fig. S17).

[3] The "coxal" values are estimates from the acetabular heights of the associated coxal bones (Thibeault and Villotte, 2018).

[4] The body mass estimates employ an average of the Alpha femoral head diameter estimates (47.65 mm), and the femoral head derived measurements for Beta and Gamma (42.2 mm and 49.4 mm respectively) [body mass = 2.262 x FemHd – 38.7 (Ruff et al., 2018)].

Table S5. Osteometric dimensions of the proximal and distal Cro-Magnon femora, in millimeters and degrees.

	M#	***Beta Right 4321***	***Beta Left 4329***	***Gamma Right 4328***	***Gamma Left 4322***
Vertical head diameter	18	41.7			(49.4)[1]
Transverse head diameter	19	42.2			
Vertical neck diameter	15				37.3
Neck-shaft angle	29				(129°)[2]
Epicondylar breadth	21		75.4		
Bicondylar breadth			67.0		
Medial condyle A-P			60.9	(65.0)	
Lateral condyle A-P			63.2	(66.5)	
Medial condyle breadth	21c		(26.5)		
Lateral condyle breadth	21e		29.0	(31.0)	
Intercondylar breadth			14.9	30.8	
Medial condyle height	26		35.0	39.0	
Lateral condyle height	25		36.0	36.0	
Medial patellar projection			58.0	63.6	
Lateral patellar projection	22		61.4	64.6	
Patellar facet height			36.7	36.6	
Patellar facet breadth			40.4	(42.3)	
Patellar facet medial breadth			17.0		
Patella facet lateral breadth			23.4	22.3	
Bicondylar angle	30		9°	7°	

[1] The CM 4322 femoral head diameter is estimated by completing the contour of the preserved partial head articulation (Thibeault and Villotte, 2018) (see Fig. S17 and Table S4).

[2] The CM 4327 (Alpha) right femur preserves only the medial neck, which indicates a neck-shaft angle similar to or slightly higher than that of CM 4322 (Fig. S19).

3. The Cro-Magnon Tibial Remains

3.1 The Cro-Magnon Tibiae

Portions of four tibiae are preserved from Cro-Magnon, CM 4330 to CM 4333 (Figs. S21 to S24; Tables S6 to S8). The first of these is an essentially complete tibia, one of the most complete long bones from Cro-Magnon. The others consist of a largely complete diaphysis (CM 4332) and two tibiae from near midshaft to the distal epiphysis (CM 4331 and 4333). Following Thibeault and Villotte (2018) (Table S1), the CM 4331 and 4332 are part of the Alpha postcrania (and by extension Cro-Magnon 1) and CM 4330 and 4333 belong with the Gamma postcrania.

The Cro-Magnon tibiae were extensively discussed by Broca (1868), and especially the CM 4332 diaphysis (which he attributed to Cro-Magnon 1). He was especially impressed by the "disposition en lame de sabre" (extreme platycnemia), which he saw as a consequence of an anteroposterior diaphyseal expansion combined with a mediolateral flattening. A similar interpretation was expressed by Pruner-Bey (1868). However, as noted and illustrated by Vallois and Billy (1965), the cnemic indices of these tibiae are not especially low, and the anterior crests are less sharp than was implied by Broca (see Fig. S25). Moreover, the extremely platycnemic tibia illustrated by Broca (1868) was not even from Cro-Magnon! Interestingly, despite the inclusion of retroversion and torsion angles for CM 4330 by Vallois and Billy (1965), there has been little discussion of the relatively complete proximal epiphysis of CM 4330 and the distal epiphyses of CM 4330, 4331 and 4333.

Figure S21. The Cro-Magnon tibiae in anterior view. CM 4330 and 4331 are left, whereas CM 4332 and 4333 are right. Aligned approximately with respect to their distal epiphyses.

Figure S22. The Cro-Magnon tibiae in posterior view. CM 4330 and 4331 are left, whereas CM 4332 and 4333 are right. Aligned approximately with respect to their distal epiphyses.

Figure S23. The Cro-Magnon tibiae in medial view. CM 4330 and 4331 are left, whereas CM 4332 and 4333 are right. Aligned approximately with respect to their distal epiphyses.

Figure S24. The Cro-Magnon tibiae in lateral view. CM 4330 and 4331 are left, whereas CM 4332 and 4333 are right. Aligned approximately with respect to their distal epiphyses.

3.2. Tibia Right 4332 (Alpha)

3.2.1 Preservation

The tibia retains the essentially complete diaphysis. Proximally it has an irregular transverse break at level of proximal tibial tuberosity anteriorly and at the proximal end of the soleal line posteriorly. Distally it ends at the level of the proximal fibular syndesmosis. The diaphysis in between is intact with only surface abrasion from 150 years of handling.

3.2.2 Morphology

Proximally the tibial tuberosity is minimally rugose near the proximal break, and it has only a slight indentation at its distal end (Figs. S21 and S24). There is a small lip, partly abraded, on the lateral tibial tuberosity edge, accentuating the proximal end of the concavity between the anterior crest and the interosseus line.

The interosseus line is raised and sharp along the proximal half of shaft, and it then becomes rugose to the distal end (Fig. S24). There is a wide sulcus between the anterior crest and the interosseus line along the proximal half of the diaphysis, being most pronounced between the mid-proximal shaft and midshaft. The anterior crest is prominent but rounded (Fig. S25); it lacks the sharpness implied by Broca's "lame de sabre."

The strongly evident soleal line (Fig. S26) is smooth for its proximal ≈20 mm, and then it becomes a raised rugose area 10-15 mm wide across the mid-posterior crest, at the proximal end of the pilaster. The soleal line then remains moderately rugose distally, ≈5 mm wide, to the medial side. It rises onto a small crest that largely fades out by midshaft, but the rugosity along the posteromedial side of the shaft continues to the level of the minimum circumference.

Figure S25. Midshaft (50%) cross-sections of the Cro-Magnon tibiae and fibulae. Anterior is above. The CM 4330 left tibia is as viewed from proximal; the CM 4332 right tibia and the CM 4334 and 4335 right fibulae section are reversed so that lateral is on the left for all four sections. The scale is 1 cm square.

Figure 26. Posterior views of the proximal diaphyses of the CM 4330 left tibia and the CM 4332 right tibia. The view of CM 4330 is directly posterior; the one of CM 4332 is slightly posteromedial. Scale bar: 5 cm.

Running down the mid-posterior diaphysis, from the nutrient foramen to near midshaft, is a prominent and strongly marked tibial pilaster (*sensu* McCown and Keith, 1939) (Fig. S26); it is most evident in medial view (Fig. S27). It is slightly oblique from proximomedial to distolateral. It exhibits a rugose flexor line (between the origins of tibialis posterior and flexor digitorum longus) for ≈45 mm down the middle of the pilaster.

On the proximal posterior shaft, between the soleal line and the medial side, there is a roughening of the surficial bone down from the capsular area at the pes anserinus insertion area, for up to ≈40 mm from the proximal break. It exhibits at least one oblique line parallel to the soleal line (Fig. S26).

There is a moderately marked rugosity for the distal tibiofibular ligament, but the bone does not extend sufficiently distally to assess its full development.

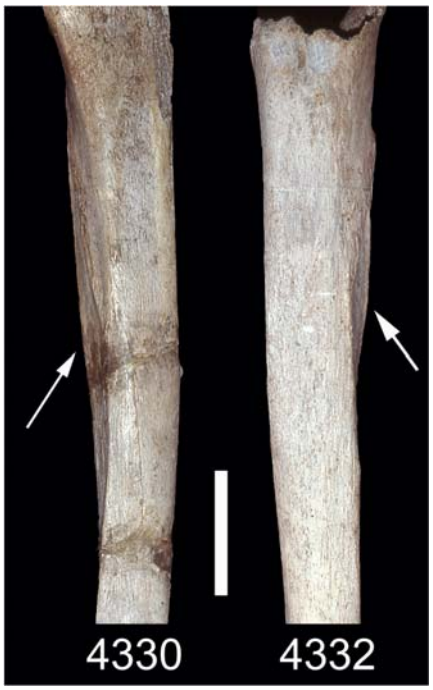

Figure S27. Medial views of the CM 4330 and 4332 mid-proximal tibial diaphyses, with the prominent tibial pilasters (especially of CM 4330) indicated. Scale bar: 5 cm.

3.2.3 Paleopathology

Of uncertain etiology or significance, there are two vascular grooves between the anterior crest and the interosseus line. The more prominent one is at the mid-distal level. There is a groove ≈0.5 mm wide extending from the anterior crest two-thirds of the way to the interosseus line for 15.3 mm. It has a raised ridge along the proximal side and a smaller one on the distal side. The other groove is fainter and more proximal, ≈20 mm distal of midshaft. It is oblique from the anterior crest proximally to the interosseus line distally, but it is mostly horizontal. It is apparent by the anterior crest for ≈10 mm, it largely fades through the anterolateral concave area, and then it becomes apparent for ≈10 mm to and across the interosseus line. At the interosseus line, it interrupts the rugosity of the line.

3.3 Tibia Left 4331 (Alpha)

3.3.1 Preservation

The partial tibia retains the distal half of the shaft from just proximal of midshaft to the distal epiphysis. The distal epiphysis has abrasion across all of the anterior portion, including the anterior edges of the trochlear and malleolar surfaces, the anterolateral corner and the anterior surface of the medial malleolus. The remainder of the distal epiphysis is intact with minor abrasion to the other margins.

3.3.2 Morphology

The partially preserved midshaft has a rounded anterior crest, and the interosseus line is angled but not rugose. There is a distinct rugosity along the anterior crest for ≈50 mm from the proximoanterior break near midshaft. Otherwise the shaft is mostly featureless.

Distally the trochlear and malleolar facets are smooth (Fig. S28C). The abrasion to the anterior margin prevents assessment of whether squatting facets were present. The flexor hallucis longus / tibialis posterior bursa sulcus is slightly irregular, has a proximal medial lip, but blends laterally with the epiphyseal surface (Fig. S28A). There are minor irregularities for the distal attachment of the interosseus membrane, including a small knob (Fig. S28B), as part of the distal tibiofibular syndesmosis.

In the anterior corner of the trochlear-malleolar juncture, there is a shallow and rounded depression 7.1 mm anteroposterior and 3.5 mm mediolateral (Fig. S28C); it is larger and shallower than the one on CM 4330 (see 3.4.2 below), but in the same location.

3.3.3 Paleopathology

At the posterior side of the distal fibular area, there is a knob of bone which is a continuous extension of the posterior epiphyseal surface (Fig. S28). It swells modestly posteriorly but projects markedly laterally. The lateral edge is abraded, so its original full lateral extent is not known. The protuberance is 20.6 mm proximodistal; it is 11.7 mm anteroposterior at its base and 7.5 mm at its preserved lateral extent; it projects ≈9 mm from the middle of the fibular surface. It is in the position of the posterior tibiofibular ligament, and it is likely to be a partial ossification of that ligament; the distal right fibula is not preserved for Alpha, and therefore whether there was ossification to the fibula is not known.

There is a moderate osteophytic lip to the margin of the malleolar articular surface and the posterior margin of the trochlea. At the posterior edge of lateral half of the trochlear surface, there are two resorptive holes. The shallow hole is 2.7 mm in diameter, and a larger one is 3.2 mm in diameter. The latter hole opens down into rounded trabeculae, and there is a greater diameter for the internal lesion than for the opening, implying a form of cyst.

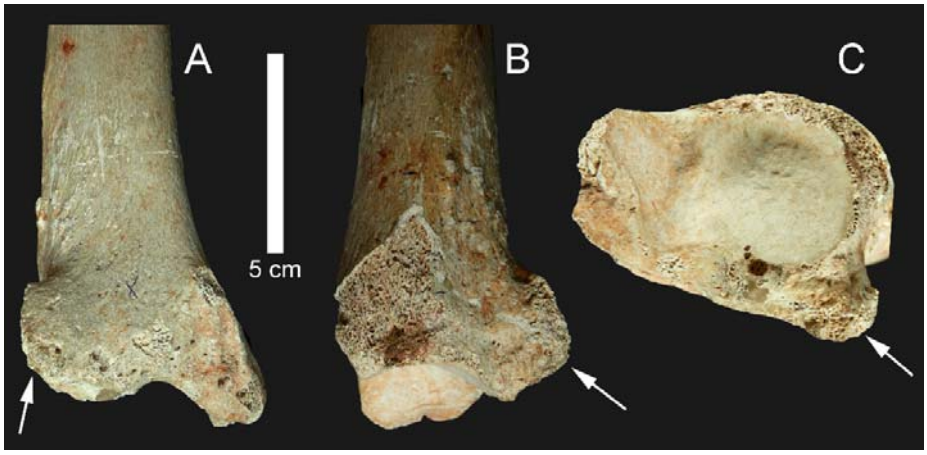

Figure S28. The distal epiphysis of the CM 4331 left tibia in posterior (A), lateral (B), and distal (C) views. The arrows indicate the posterolateral protuberance on the epiphysis, in the region of the posterior tibiofibular ligament. Scale is for A and B; C is enlarged relative to A and B.

As with CM 4332, there are two vascular grooves on the diaphysis. The more proximal one is 42 mm distal of proximoanterior break (≈ midshaft). It extends perpendicular to the shaft axis across the lateral anterior crest to the mid-lateral sulcus for 16.4 mm. It cuts through the modest rugosity on the anterior crest, and it is most prominent (deepest and widest) for 5.6 mm just onto the lateral surface from the anterior crest rounding. The second

vascular groove is near the distal minimum circumference; its sulcus is ≈20 mm long from the anterior crest almost to the interosseus line. It is maximally ≈1.5 mm wide. Its orientation is primarily anteroposterior, but it is slightly anteromedioproximal to posterolaterodistal.

3.4 Tibia Left 4330 (Gamma)

3.4.1 Preservation

The tibia is complete with abrasion to the epiphyseal margins, especially proximally (Figs. S21 and S22). As such, it is the most complete of the Cro-Magnon long bones, approached in completeness only by the CM 4297 ulna and its associated CM 4334 fibula. The proximal epiphysis lacks the anterior surface of the tibial tuberosity and the anterior margins of the intercondylar space and the medial condyle. Only the lateral condyle is preserved to its anterior margin. There is minor abrasion to the posterior lateral condyle and more extensive damage to the posterior medial condyle, with three holes into the trabeculae.

The diaphysis is largely complete with a clean glue join midshaft and a less clean join with some bone loss mid-distally. There is also a clean but reglued break just proximal of the distal epiphysis. The distal epiphysis is intact with surface abrasion to the posterolateral epiphysis and the anterior half of the lateral epiphysis.

3.4.2 Morphology

Proximally, the articular surfaces are normal with a moderately strong torsion (20°). The tibial plateau exhibits modest retroversion angles (10° on the medial condyle), values which are at the bottoms of the Late Pleistocene sample variations. It is matched only by the (pathological) Dolní Věstonice 15 among the MUP tibiae, plus Oberkassel 1 and Ohalo 2 in the LUP sample (Fig. 5). The anterior intercondylar space exhibits a sulcus 4 mm wide along the medial side of the lateral condyle from the intercondylar spine. The posterior intercondylar space has a depression 3.5 mm in diameter just posterior of the medial intercondylar spine.

On the proximal diaphysis there is a weak soleal line with a maximum breadth of ≈9 mm, which nonetheless remains rugose to its distomedial edge. The tibial pilaster is present with a posterior angulation along the proximal shaft from the soleal line to midshaft (Fig. 27). However, it does not stand out from the adjacent shaft, being more of an angulation of the posterior angle of the shaft (rather than rounded) (Fig. S26). There is a sharp interosseous crest from the proximal epiphysis and the proximal fibular facet to the mid-distal shaft. The anterior crest is moderately angled (Fig. S25).

There are few changes in the area of the distal tibiofibular syndesmosis. There is a weakly marked flexor hallucis longus / tibialis posterior bursa sulcus, albeit with a raised and roughened medial margin 2.5 mm wide.

The distal trochlear and malleolar articular surfaces are normal (Fig. S29). There is a small pit near the anterior articular edge where the trochlear and malleolar facets meet, ≈1.5 wide, with articular bone between it and the anterior edge of the trochlear surface. Anterior to that pit there is a small raised crest at the margin of the articular surface.

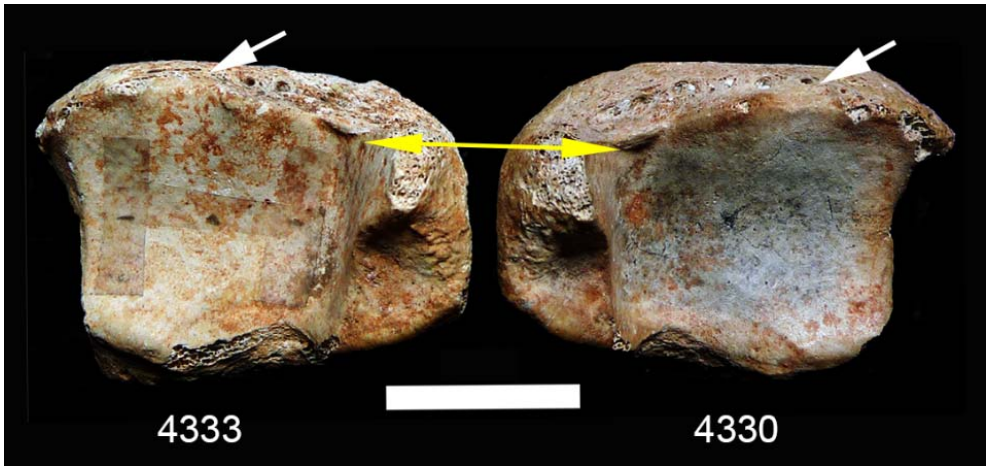

Figure S29. Distal views of the CM 4330 and 4333 tibiae. White arrows: anterolateral trochlear rounding / squatting facets. Yellow arrow: anteromedial articular pit on CM 4330 and the small bridging crest on both tibiae. Scale bar: 2 cm.

In addition, laterally there is a distinct anterior rounding of the articular border (Figs. 6 and S29). It is lunate shaped, extending 3.2 mm from the trochlear surface with a maximum width of 11.5 mm. It is more of a rounding of the articular edge than a full squatting facet (see Trinkaus, 1975), but it articulates with the distinct squatting facet on the CM 4337 left talus. It is therefore scored as a squatting facet (Table S8), and it reinforces the habitual pedal dorsiflexion inferred from the Cro-Magnon pedal remains (Trinkaus et al., 2021b). There is no evidence of a similar rounding on the medial anterior margin. The anterior surface adjacent to the facet exhibits six foramina into the underlying trabeculae.

3.4.3 Paleopathology

None of the CM 4330 articular surfaces exhibit abnormal changes. However, there is a vascular groove of uncertain etiology on the proximolateral shaft 124 mm from the lateral condyle, extending from just lateral of the anterior crest for 30 mm and perpendicular to the shaft axis. It is up to 1.0 mm wide and most evident along the first 15.2 mm from the anterior crest. It continues on either side of the interosseus line/crest; it does not interrupt the interosseus line.

3.5 Tibia Right 4333 (Gamma)

3.5.1 Preservation

The bone retains the mid-distal and distal diaphysis plus the distal epiphysis. The proximal end was broken off modestly distal of midshaft and then further eroded; it does not extent as far proximally as midshaft, and hence the absence of diaphyseal diameters for it (Table S6).

There is a fossilization crack down the lateral side midway between the interosseus line and the anterior crest to the distal minimum circumference area. The distal epiphysis is largely present, but it exhibits abrasion to the anterior side of the fibular area and erosion to the anterior area above the malleolus; neither area of damage affects either the distal articulations or the musculoligamentous markings.

3.5.2 Morphology

The diaphysis exhibits the distal end of what was likely a prominent pilaster more proximally. The posteromedial border and the interosseus line are both sharp and angled to the distal epiphysis. The distal tibiofibular ligamentous markings are hardly a rugosity, even less so than on CM 4330.

As with CM 4330, there is no evidence of a squatting facet distoanteromedially, but the distoanterolateral margin has a distinct rounding of the border (Figs. 6 and S26). It exhibits a lunate shape 4.1 mm from trochlear surface with a maximum breadth of 10.7 mm. As with the similar area on CM 4330, it is more of an extended rounding than a full squatting facet, but it is scored as squatting facet (Table S8). There are five small foramina above the area of squatting facets anteriorly.

On the anteromedial corner of the trochlear articulation, where it meets the malleolar facet, there is a tiny crest bridging the angle (Fig. S29). It is similar to the small crest on CM 4330, but there is none of the pit present on CM 4330 and CM 4331.

The flexor hallucis longus / tibialis posterior sulcus is largely smooth with some porosity. There is a raised ridge along its proximomedial portion, similar to the one on CM 4330 but not as prominent.

3.5.3 Paleopathology

There are no apparent lesions on the bone.

Table S6. Lengths and diaphyseal dimensions of the Cro-Magnon tibiae, in millimeters.

	M#	***Alpha Right 4332***	***Alpha Left 4331***	***Gamma Right 4333***	***Gamma Left 4330***
Maximum length	1a	(394.2)[1]			382.0
Total length medial	1b	(383.6)[2]			374.8
Total length lateral	1	(386.3)[2]			375.0
Articular length medial	2	(369.3)[2]			358.5
Articular length lateral		(372.0)[2]			358.7
Biomechanical length[3]		(370.7)			358.6
Midshaft anteroposterior diameter	8	36.2	36.0		37.2
Midshaft mediolateral diameter	9	25.5	24.6		26.3
Midshaft circumference	10	100.0	97.5		95.5
Proximal anteroposterior diameter	8a	45.8			41.5
Proximal mediolateral diameter	9a	27.0			26.5
Proximal circumference	10a	115.5			106.0
Distal minimum circumference	10b	89.0	89	84	86.5
Flexor line[4]		present			present

Notes to Table S6

[1] The maximum length of the CM 4332 tibia was estimated by matching surface renderings of the preserved portions of the tibia to renderings of five Upper Paleolithic individuals (Thibeault and Villotte, 2018).

[2] The medial and lateral total lengths and the medial and lateral articular lengths of CM 4332 were estimated from its maximum length using least squares regressions based on a recent human geographically diverse sample (n = 63) (Stringer et al., 1998; Shang and Trinkaus, 2010) (MedTotLen = 0.967 x Len + 2.4, r^2 = 0.992; LatTotLen = 0.975 x Maxlen + 1.9, r^2 = 0.993; MedArtLen = 0.933 x MaxLen + 1.6, r^2 = 0.981; LatArtLen = 0.941 x MaxLen + 1.0, r^2 = 0.981).

[3] Biomechanical length is the average of the medial and lateral articular lengths (Ruff and Hayes, 1983).

[4] Presence of a distinct crest, along the tibial pilaster distally from the soleal line, between the tibialis posterior and flexor digitorum longus muscle origins.

Table S7. Midshaft cross-sectional geometric parameters of the Cro-Magnon tibiae.[1]

	Alpha Right 4332	***Gamma Left 4330***
Total area	698.8	631.6
Cortical area	534.1	522.2
A-P 2nd moment of area (Ix)	56715[2]	48247
M-L 2nd moment of area (Iy)	29884[2]	23479
Max. 2nd moment of area (Imax)	63523	50228
Min. 2nd moment of area (Imin)	23076	21498
Polar moment of area (J,Ip)	86599	71726
A-P section modulus (Zx)[3]	2903	2413
M-L section modulus (Zy)[3]	2018	1552
Polar section modulus (Zp)[3]	4294	3466

[1] Although the CM 4331 tibia is sufficiently intact to provide midshaft diameters (Table S6), it is too damaged to provide a reliable midshaft cross-section (Fig. S22).

[2] The CM 4332 tibia is oriented such that the anterolateral surface at the mid-proximal level is parasagittal, which approximates the anatomical orientation for Ix and Iy.

[3] The section moduli are calculated from the second moments of area and diaphyseal diameters based on Trinkaus and Ruff (2012).

Table S8. Osteometric dimensions of the proximal and distal Cro-Magnon tibiae, in millimeters and degrees.

	M#	*Alpha Left 4331*	*Gamma Right 4333*	*Gamma Left 4330*
Proximal maximum breadth	3			78.0
Medial condyle breadth	3a			(30.0)
Lateral condyle breadth	3b			36.0
Lateral condyle depth	4b			43.5
Intertubercular distance[1]				10.0
Tuberosity projection[2]				(40.0)
Medial retroversion angle	12			10°
Lateral retroversion angle				12°
Medial inclination angle	13			8°
Lateral inclination angle				10°
Torsion angle[3]	14			20°
Distal maximum breadth	6	55.0	53.5	53.5
Distal epiphyseal depth	7	(42.0)	38.5	38.1
Distal articular breadth[4]		31.5	30.0	30.8
Medial articular depth[5]		25.0	24.3	22.0
Lateral articular depth[6]			29.5	31.3
Medial squatting facet			absent	absent
Lateral squatting facet			present	present

[1] Distance between the tibial spines. Vančata (1991) measurement 53.

[2] Distance from the anterior tibial tuberosity to the anteroposterior middles of the tibial condyles, measured perpendicular to the diaphyseal axis (Trinkaus and Rhoads, 1999).

[3] Measurement from Vallois and Billy (1965).

[4] Distance between the lateral middle of the trochlear surface and the middle of the angle between the trochlear and malleolar surfaces.

[5] Minimum medial anteroposterior dimension of the trochlear surface.

[6] Maximum lateral anteroposterior dimension of the trochlear surface.

4. The Cro-Magnon Fibular Remains

4.1 The Cro-Magnon Fibulae

There are two fibulae preserved in the Cro-Magnon sample, the proximal half of a right diaphysis that is attributed to Alpha (CM 4335) and a largely complete right bone attributed to Gamma (CM 4334) (Figs. S25 and S30). A virtual mirror image of the CM 4334 fibula provides an excellent match to the CM 4330 tibia (Thibeault and Villotte, 2018: Fig. 6). CM 4335 is attributed to Alpha given its larger dimensions and its duplication with CM 4334 (both are right).

4.2 Fibula Right 4335 (Alpha)

4.2.1 Preservation

The bone retains the diaphysis from the distal end of the neck to slightly distal of midshaft. The section is intact except for minor erosion on the anterior crest just distal of the neck and the posteromedial edge near midshaft.

4.2.2 Morphology

CM 4335 is a larger and more substantial bone than CM 4334 (Fig. S30; Table S9). The soleal line is a strongly rugose strip on the proximoposterior shaft, up to 9.5 mm wide and 58 mm long. The lateral sulcus is strongly concave, especially in the mid-proximal area (Figs. S25 and S30); its dimensions at its maximum development are: shaft anteroposterior: 17.9 mm; shaft mediolateral: 14.4 mm; sulcus chord: 12.4 mm; sulcus depth: 5.0 mm.

The anterior crest has a flattened area on its medial side, up to 7 mm wide, which then angles to a broader area along most of the medial surface. The larger medial surface is mostly flat in its more proximal portion, but it then becomes concave towards midshaft (sulcus chord: 13.3 mm; sulcus depth subtense: 1.6 mm; measured at the maximum sulcus development and more distally than the lateral sulcus measurements.

4.2.3 Paleopathology

There are no apparent lesions on the bone.

Figure S30. The Cro-Magnon 4334 and 4335 right fibulae in medial (left) and lateral (right) views. Scale bar: 5 cm.

4.3 Fibula Right 4334 (Gamma)

4.3.1 Preservation

The bone is essentially complete, from the proximal styloid process to the distal one, with abrasion to each tip. There are three reglued breaks on the shaft, leading to a slight (1-2 mm) expansion.

The proximal shaft break is just distal of the neck 90-110 mm from proximal tip, with wax infilling along the anterior crest. The other breaks are clear transverse ones, 240 mm and 300 mm from the proximal end. The proximal epiphysis sustained abrasion to the styloid process and erosion into the trabeculae on the anterior articular and epiphyseal surfaces and on the posteroinferior articulation. Distally, all of malleolar facet and digital fossa are present, with minor abrasion to the anterior edge of the malleolar facet; almost all of the lateral epiphyseal surface was eroded away.

4.3.2 Morphology

Proximally where preserved, the ligamentous surfaces are smooth and undulating. The articular facet is smooth superiorly but uneven anteriorly (see below). The soleal line, rather than a proximal rugosity, is a sharp posteromedial crest, ≈29 mm long. At the distal end of the neck, centered ≈60 mm from the proximal end, there is a rugose hollow 5.7 mm wide and 0.8 mm deep along its posterior side.

The shaft is dominated by a large, sharp and prominent anterior crest and the associated lateral sulcus (Figs. S25 and S30). The crest is most prominent just distal of the neck, and then it gradually reduces distal of midshaft. At the maximum development of the crest, ≈160 mm distal of the proximal end, the measurements are: shaft anteroposterior: 17.2 mm; shaft mediolateral: 12.1 mm; lateral sulcus chord: 17.7 mm; lateral sulcus subtense depth: 3.8 mm. On the medial surface there is a rugose area along the maximum crest development, but it is otherwise flat. It becomes modestly concave at the level of the maximum lateral crest: sulcus chord: 11.2 mm; sulcus depth subtense: 1.4 mm.

The nutrient foramen has its subperiosteal opening ≈175 mm from the proximal end. It leads into a proximally extending vascular sulcus that extends for ≈24 mm from the opening. It is a distinct sulcus with sharply curving-over edges enclosing it, especially on its distal half.

There is nothing special for the distal epiphysis and talar articulation. The distal tibiofibular ligamentous attachments consist of a strong and rugose ridge, along with an anterior crest to the proximoposterior corner of the malleolar surface. It creates a fossa 3.6 mm long along the anterior edge of the ridge, such that the ligamentous area is both depositional and resorptive.

4.3.3 Paleopathology

The inferior 8.8 mm of the proximal articular facet is roughened and porous, more of an irregularity and elevation of the facet than the laying down of additional bone. There are no associated changes on the proximal fibular facet of the CM 4330 tibia; however, that tibia is left, and the proximal end of the right tibia (CM 4333) is absent.

Table S9. Osteometric dimensions of the Cro-Magnon fibulae, in millimeters.

		Alpha Right 4335	***Gamma Right 4334***
Maximum length	1		(375.0)
Articular length	1a		(365.0)
Midshaft maximum diameter	2	19.8	18.5
Midshaft minimum diameter	3	15.9	10.3
Midshaft circumference	4	57.5	48.5
Midshaft anteroposterior diameter	3(2)		17.3
Midshaft mediolateral diameter	3(1)		12.3
Neck maximum diameter		14.5	12.2
Neck minimum diameter		10.9	10.3
Neck circumference		44.0	33.0
Neck anteroposterior diameter			10.8
Neck mediolateral diameter			10.7
Proximal anteroposterior diameter			27.5
Proximal mediolateral diameter	4(1)		20.8
Distal shaft anteroposterior diameter			16.1
Distal shaft mediolateral diameter			14.0
Distal shaft circumference			43.5
Distal epiphyseal depth			27.3
Distal articular depth			(24.5)
Distal articular height			29.0

5. Comparative Samples

Sites in the comparative samples providing data for the osteometric, discrete trait, cross-sectional geometry and geometric morphometric assessments of the Cro-Magnon femora and tibiae. Southwest Asian specimens are indicated by an asterix.

Neandertals (Late Pleistocene):

Amud*, La Chaise-Tour, La Chapelle-aux-Saints, Feldhofer, La Ferrassie, Font-de-Forêt, Kebara*, Kiik-Koba, Krapina, Oliveira, Palomas, Pofi, Les Pradelles, La Quina, Regourdou, Rochers-de-Villeneuve, Saint Césaire, Santa Croce, Shanidar*, El Sidrón, Spy, Stadel, Tabun*, Zafarraya

Middle Paleolithic modern humans:

Qafzeh*, Skhul*

Early/Mid Upper Paleolithic humans:

Barma Grande, Baousso da Torre, Caviglione, Dolní Věstonice I and II, Grotte des Enfants, Mittlere Klause, Mladeč, Nahal Ein Gev*, Ostuni, Paglicci, Pataud, Paviland, Pavlov I, Předmostí, La Rochette, Sunghir, Veneri/Parabita, Willendorf

Late Upper Paleolithic humans:

Arene Candide, Balzi Rossi, Bichon, Cap Blanc, Chancelade, Climente, Continenza, Ein Gev*, Karaneh*, Lafaye, Laugerie Basse, La Madelaine, Maritza, Mataha*, El Mirón, Neve David*, Oberkassel, Ohalo II*, Le Peyrat, Riparo Tagliente, Le Roc, Rochereil, La Rochette, Romanelli, Romito, Saint Germain-la-Rivière, San Teodoro, Vado all'Arancio, Villabruna,

6. Comparative Femoral and Tibial Values and Indices

Table S10. Crural indices ((tibial maximum length / femoral bicondylar length) x 100) for Cro-Magnon Alpha and Gamma. and Late Pleistocene samples [mean ± SD (n)].[1]

Cro-Magnon Alpha	80.8
Cro-Magnon Gamma	80.3
Neandertals	78.8 ± 2.1 (8)
MPMH	89.6 (1)
E/MUP	84.9 ± 2.0 (19)
LUP	85.3 ± 2.2 (20)

[1] MPMH: Middle Paleolithic modern humans; E/MUP: Early and Mid Upper Paleolithic modern humans; LUP: Late Upper Paleolithic modern humans.

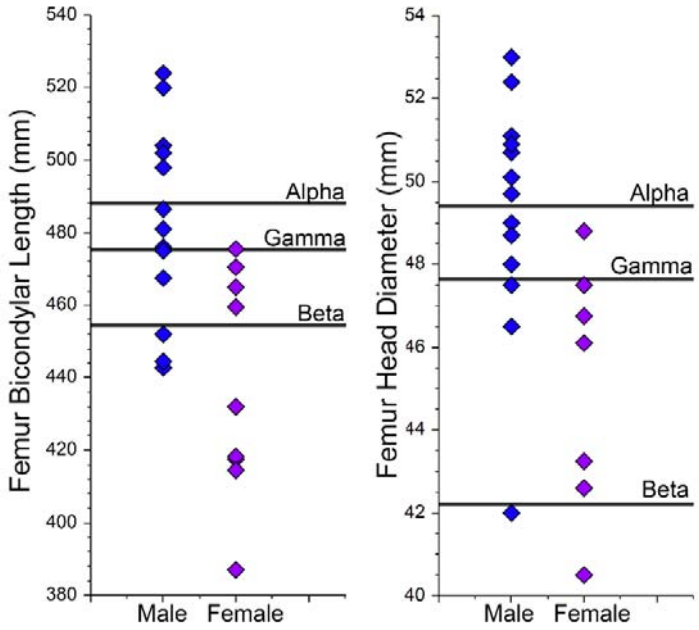

Figure S31. Comparison of the Cro-Magnon femoral lengths and head diameters (as reflections of stature and body mass) versus those for reliably sexed E/MUP males and females.

Table S11. Femoral and tibial diaphyseal indices for Cro-Magnon and comparative Late Pleistocene samples [mean ± SD (n)].[1]

Femur	***Meric Index***	***Pilastric Index***
Cro-Magnon		
Alpha CM 4327 Right	83.2	129.5
Alpha CM 4325 Left	76.5	125.3
Beta CM 4324 Left		124.1
Gamma CM 4323 Right	70.8	
Gamma CM 4322 Left	72.3	118.5
Neandertals	79.5 ± 5.4 (21)	100.9 ± 9.3 (19)
MPMH	85.9 ± 12.4 (5)	122.9 ± 16.0 (9)
E/MUP	75.7 ± 6.8 (31)	118.1 ± 11.1 (28)
LUP	77.9 ± 6.4 (29)	116.0 ± 9.5 (30)

Tibia	***Cnemic Index***	***Midshaft Index***
Cro-Magnon		
Alpha CM 4332 Right	169.6	142.0
Alpha CM 4331 Left		146.3
Gamma CM 4330 Left	156.3	141.4
Neandertals	143.4 ± 12.6 (10)	140.9 ±11.4 (14)
MPMH	157.7 ± 9.5 (5)	143.9 ± 10.1 (8)
E/MUP	161.0 ± 14.5 (25)	150.3 ± 17.8 (23)
LUP	166.4 ± 20.0 (25)	150.9 ± 17.6 (21)

[1] MPMH: Middle Paleolithic modern humans; E/MUP: Early and Mid Upper Paleolithic modern humans; LUP: Late Upper Paleolithic modern humans.

7. Geomorphometric Comparisons of Femoral Contours

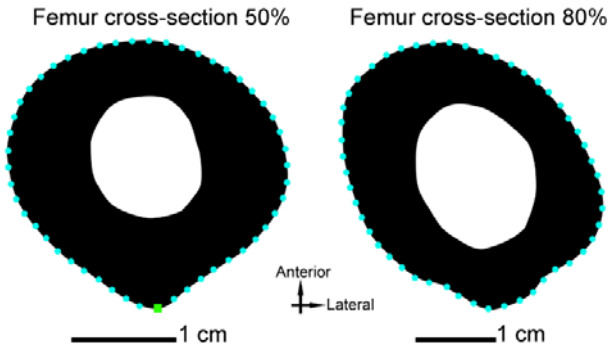

Figure S32. Femoral midshaft (50%) and subtrochanteric (80%) sections with the landmark (green square) and semi-landmarks (cyan circles) indicated.

In addition to the standard of minimizing the Procrustes distance between corresponding points when sliding the semi-landmarks, we also used the criterion of minimizing the bending energy [BE, see Zelditch et al. (2004) for more information]. The

results using the standards of Procrustes distance indicate that the distances between each two semi-landmarks along the cross-sectional contour could be inconsistent in some cases, and that this non-shape element might affect the shape relationships among different specimens. Therefore, we performed the superimposition analysis again minimizing the BE as the criterion during the sliding of the semi-landmarks. According to the results, the BE standards could reduce this inconsistency between the two curve semi-landmarks. The resultant relative positions of the fossils remain similar between the two analyses (compare Figs. 9 and 10 with Figs. S33 and S34).

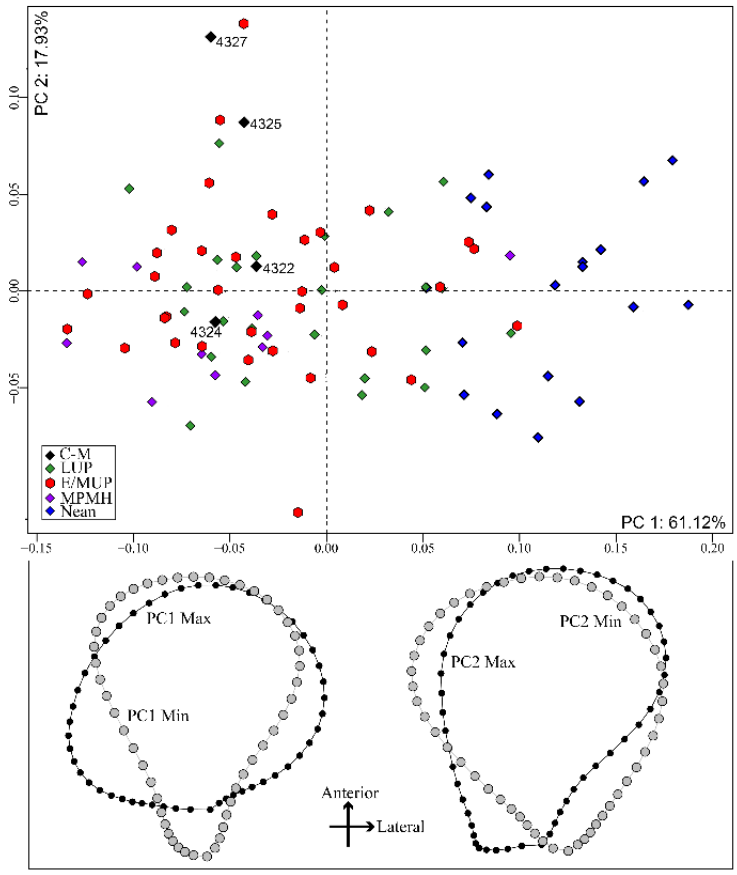

Figure S33. Principal component (PCA) analysis of the bending energy standards for Cro-Magnon and comparative Late Pleistocene femoral midshaft (50%) contours.

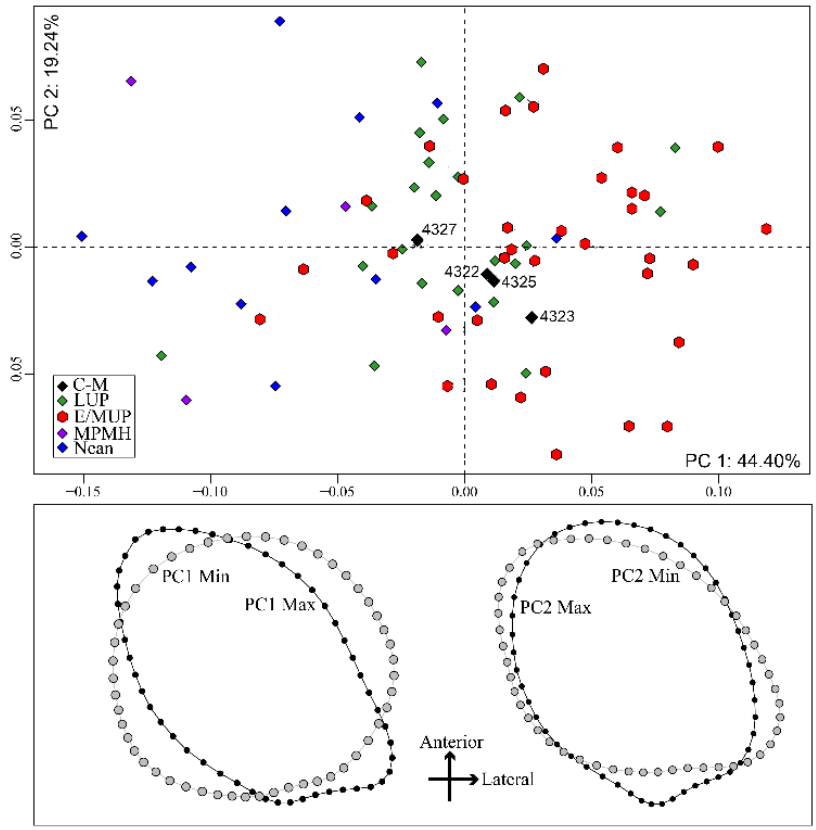

Figure S34. Principal component (PCA) analysis of the bending energy standards for Cro-Magnon and comparative Late Pleistocene femoral subtrochanteric (80%) contours.

8. Supporting Information References

Bolanowski, W., Śmiszkiewicz-Skwarska, A., Polguk, M., Jędrzejewski, K.S., 2005. The occurrence of the third trochanter and its orrelation to certain anthropometric parameters of the human femur. Folia Morphologica 64, 168-175.

Broca, P., 1868. Sur les crânes et ossements des Eyzies. Bull. Soc. Anthropol. Paris 3, 350–392. https://doi.org/10.3406/bmsap.1868.9548

Dastugue, J., 1967. Pathologie des hommes fossiles de l'Abri de Cro-Magnon. L'Anthropol. 71, 479-492.

Fu, Q., Mittnik, A., Johnson, Philip L.F., Bos, K., Lari, M., Bollongino, R., Sun, C., Giemsch, L., Schmitz, R., Burger, J., Ronchitelli, Anna M., Martini, F., Cremonesi, Renata G., Svoboda, J., Bauer, P., Caramelli, D., Castellano, S., Reich, D., Pääbo, S., Krause, J., 2013. A revised timescale for human evolution based on ancient mitochondrial genomes. Curr. Biol. 23, 553–559.

Henry-Gambier, D., 2002. Les fossiles de Cro-Magnon (Les Eyzies-de-Tayac, Dordogne): nouvelles données sur leur position chronologique et leur attribution culturelle. Bull. Mém. Soc. Anthropol. de Paris 14, 89-112.

Houzé, E., 1883. Sur la présence du troisième trochanter chez I'homme. Bull. Soc. Anthropol. Bruxelles. 2, 21-52.

Hrdlička, A., 1934. The hypotrochanteric fossa of the femur. Smithsonian Misc. Coll. 92, 1-49.
Hrdlička, A., 1937. The gluteal ridge and gluteal tuberosities (3rd trochanters). Am. J. Phys. Anthropol. 23, 127-198.
Laine, A. 1895. "Abri sous roche de Cro-Magnon. Mission L. Lartet". [Os]. Plaque provenant de la collection de plaques de projection du Musée de l'Homme. PV0059396. Paris: Musée de l'Homme. https://www.quaibranly.fr/fr/explorer-les-collections/base/Work/action/show/notice/908729-abri-sous-roche-de-cro-magnon-os/page/2/.
McCown, T.D., Keith, A., 1939. The Stone Age of Mount Carmel II: The Fossil Human Remains from the Levalloiso-Mousterian. Oxford: Clarendon Press.
Pruner-Bey, F., 1868. An account of the human bones found in the cave of Cro-Magnon, in Dordogne, in: Lartet, E., Christy, H. (Eds.), Reliquiae Aquitanicae: Being Contributions to Archaeology and Palaeontology of Périgord and the Adjoining Provinces of Southern France (1865-75). Williams and Norgate, London, pp. 73–92.
Resnick, D., Greenway, G. 1982. Distal femoral cortical defects, irregularities, and excavations. Radiology 143, 345-354. http://doi.10.1148/radiology.143.2.7041169.
Ruff, C.B., Hayes, W.C., 1983. Cross-sectional geometry of Pecos Pueblo femora and tibiae – a biomechanical investigation: I. Method and general patterns of variation. Am. J. Phys. Anthropol. 60, 259-381.
Ruff, C.B., Burgess, M.L., Squyres, N., Junno, J.A., Trinkaus, E., 2018. Lower limb articular scaling and body mass estimation in Pliocene and Pleistocene humans. J. Hum. Evol. 115, 85-111. https://doi.10.1016/j.jhevol.2017.10.014.
Shang, H., Trinkaus, E., 2010. The Early Modern Human from Tianyuan Cave, China. College Station TX: Texas A&M University Press.
Stringer, C.B., Trinkaus, E., Roberts, M.B., Parfitt, S.A., Macphail, R.I., 1998. The Middle Pleistocene human tibia from Boxgrove. J. Hum. Evol. 34, 509-547. https://doi.org/10.1006/jhev.1998.0215.
Thibeault, A., Villotte, S., 2018. Disentangling Cro-Magnon: A multiproxy approach to reassociate lower limb skeletal remains and to determine the biological profiles of the adult individuals. J. Archaeol. Sci. Rep. 21, 76-86. https://doi.org/10.1016/j.jasrep.2018.06.038.
Trinkaus, E., 1975. Squatting among the Neandertals: A problem in the behavioral interpretation of skeletal morphology. J. Archaeol. Sci.. 2, 327-351. https://doi.10.1016/0305-4403(75)90005-9.
Trinkaus, E., 1976. The evolution of the hominid femoral diaphysis during the Upper Pleistocene in Europe and the Near East. Z. Morphol. Anthropol. 67, 291-319.
Trinkaus, E., Rhoads, M.L., 1999. Neandertal knees: power lifters in the Pleistocene? J. Hum. Evol. 37, 833-859. https://doi.10.1006/jhev.1999.0317.
Trinkaus, E., Ruff, C.B., 2012. Femoral and tibial diaphyseal cross-sectional geometry in Pleistocene *Homo*. PaleoAnthropology 2012, 13-62. doi 10.4207/PA.2012.ART69.
Trinkaus, E., Buzhilova, A.P., Mednikova, M.B., Dobrovolskaya, M.V., 2014. The People of Sunghir: Burials, Bodies and Behavior in the Earlier Upper Paleolithic. Oxford University Press, New York.
Trinkaus, E., Lacy, S.A., Thibeault, A., Villotte, S., 2021a. Disentangling Cro-Magnon: The dental and alveolar remains. J. Archaeol. Sci. Rep. 37, 102991. https://doi.org/10.1016/j.jasrep.2021.102911.
Trinkaus, E., Thibeault, A., Villotte, S., 2021b. Disentangling Cro-Magnon: The pedal remains. J. Archaeol. Sci. Rep. 40, 103228. doi.org/10.1016/j.jasrep.2021.103228.

Vallois, H.V., Billy, G., 1965. Nouvelles recherches sur les hommes fossiles de l'abri de Cro-Magnon. L'Anthropol. 69, 47–74.
Vančata, V., 1991. Evolution of femur and tibia in higher primates: Adaptive morphological patterns and phylogenetic diversity. Human Evolution 6, 1-47.
Villotte, S., Thibeault A., Sparacello V., Trinkaus E., 2020. Disentangling Cro-Magnon: The adult upper limb skeleton. J. Archaeol. Sci. Rep. 33, 102475. https://doi.org/10.1016/j.jasrep.2020.102475.
Zelditch, M. L., Swiderski, D. L., Sheets, H. D., & Fink, W. L. (2004). Geometric Morphometrics for Biologists: A Primer. San Diego: Elsevier Academic Press.